Protist, Vol. 169, 697–726, November 2018
http://www.elsevier.de/protis
Published online date 23 April 2018

Protist

ORIGINAL PAPER

First Ultrastructural and Molecular Phylogenetic Evidence from the Blastogregarines, an Early Branching Lineage of Plesiomorphic Apicomplexa

Timur G. Simdyanov[a,1], Gita G. Paskerova[b], Andrea Valigurová[c], Andrei Diakin[c], Magdaléna Kováčiková[c], Joseph Schrével[d,e], Laure Guillou[f], Andrej A. Dobrovolskij[b], and Vladimir V. Aleoshin[g,h]

[a]Faculty of Biology, Lomonosov Moscow State University, Leninskiye Gory 1-12, 119 234 Moscow, Russian Federation
[b]Department of Invertebrate Zoology, Faculty of Biology, Saint Petersburg State University, Universitetskaya emb. 7/9, 199 034 St. Petersburg, Russian Federation
[c]Department of Botany and Zoology, Faculty of Science, Masaryk University, Kotlářská 2, 611 37 Brno, Czech Republic
[d]CNRS 7245, Molécules de Communication et Adaptation Moléculaire (MCAM), CP 52, rue Cuvier, 75005 Paris, France
[e]Sorbonne Universités, Muséum National d'Histoire Naturelle (MNHN), UMR 7245, CP 52, rue Cuvier, 75005 Paris, France
[f]Sorbonne Université, Université Pierre et Marie Curie—Paris 6, CNRS, UMR 7144, Station Biologique de Roscoff, Place Georges Teissier, CS90074, 29688 Roscoff Cedex, France
[g]Belozersky Institute of Physico-Chemical Biology, Lomonosov Moscow State University, Leninskiye Gory 1-40, 119 234 Moscow, Russian Federation
[h]Institute for Information Transmission Problems, Russian Academy of Sciences, Bolshoy Karetny per. 19-1, 127 051 Moscow, Russian Federation

Submitted March 16, 2018; Accepted April 13, 2018
Monitoring Editor: Frank Seeber

Blastogregarines are poorly studied parasites of polychaetes superficially resembling gregarines, but lacking syzygy and gametocyst stages in the life cycle. Furthermore, their permanent multinuclearity and gametogenesis by means of budding considerably distinguish them from other parasitic Apicomplexa such as coccidians and hematozoans. The affiliation of blastogregarines has been uncertain: different authors considered them highly modified gregarines, an intermediate apicomplexan lineage between gregarines and coccidians, or an isolated group of eukaryotes altogether. Here, we report the ultrastructure of two blastogregarine species, *Siedleckia nematoides* and *Chattonaria mesnili,* and provide the first molecular data on their phylogeny based on SSU, 5.8S, and LSU rDNA sequences.

[1]Corresponding author;
e-mail simdyanov@mail.bio.msu.ru (T.G. Simdyanov).

https://doi.org/10.1016/j.protis.2018.04.006

Morphological analysis reveals that blastogregarines possess both gregarine and coccidian features. Several traits shared with archigregarines likely represent the ancestral states of the corresponding cell structures for parasitic apicomplexans: a distinctive tegument structure and myzocytotic feeding with a well-developed apical complex. Unlike gregarines but similar to coccidians however, the nuclei of male blastogregarine gametes are associated with two kinetosomes. Molecular phylogenetic analyses reveal that blastogregarines are an independent, early diverging lineage of apicomplexans. Overall, the morphological and molecular evidence congruently suggests that blastogregarines represent a separate class of Apicomplexa.

Key words: Apicomplexa; blastogregarines; ultrastructure; plesiomorphic traits; molecular phylogeny; 18S and 28S ribosomal DNAs.

Introduction

The name Apicomplexa was first introduced by Levine (Levine 1970) in order to unite "genuine" Sporozoa (gregarines, coccidians, and haemosporidians) and Piroplasmida relying on ultrastructural characters because the life cycles of the latter were poorly studied at that time and any molecular phylogenetic evidence was absent. Through the years, the composition of the group changed: in 1980, Levine moved piroplasms into Sporozoa, but simultaneously expanded the taxon (phylum) Apicomplexa, which comprised two subphyla that time: Perkinsezoa (with *Perkinsus*) and Sporozoa. Later, Perkinsezoa were consistently removed from Apicomplexa (e.g., Perkins et al. 2000), especially when *Perkinsus* was revealed to be an earliest branch of Dinozoa (Goggin and Barker 1993; Kuvardina et al. 2002), so that "Apicomplexa" was eventually reduced to "Sporozoa" and successively substituted this name, despite the fact that it was conventional during many decades before (e.g., Grassé 1953a,b). Thus, recently Apicomplexa is a junior synonym of Sporozoa in terms of the International Code of Zoological Nomenclature and consequently should be abolished. However, we support the original approach of Levine to combine Sporozoa and their closest relatives in a single taxon, and therefore, also following some recent viewpoints (e.g., Cavalier-Smith 2014; Votýpka et al. 2016), we consider Apicomplexa in this paper as a large phylogenetic clade comprising Chrompodellida (or Apicomonada in Cavalier-Smith's terminology) and Sporozoa (or Sporozoasida in Levine's terminology). Chrompodellids include free-living predatory flagellates (colpodellids) and symbiotic photosynthetic organisms (chromerids) closely related to each other (Janouškovec et al. 2015), whereas sporozoans are obligate parasites: many of them are pathogens of humans and domestic animals causing serious diseases (Perkins et al. 2000). The major sporozoan groups of high practical importance are coccidians (e.g., *Toxoplasma* and *Eimeria*), cryptosporidians, haemosporidians (e.g., *Plasmodium* causing malaria), and piroplasms (e.g., *Babesia)*, therefore these organisms are popular subjects of scientific research while gregarines and other early branching invertebrate parasites remain understudied.

Phylogenetic relationships and evolutionary history of sporozoans within Apicomplexa are still an open question. The primary divergence of sporozoans occurred most likely in marine invertebrates (Cox 1994; Leander 2008; Théodoridès 1984), which are the hosts of early branching gregarines and coccidians, as well as of some sporozoans incertae sedis that could be a source of important evidence for reconstructing the ancestral states for the Apicomplexa as a whole.

One of such unusual and poorly studied organisms are the blastogregarines – a tiny group of uncertain taxonomic affiliation encompassing intestinal parasites of marine polychaetes of the family Orbiniidae. This group comprises four species formally belonging to the single genus *Siedleckia*: *S. nematoides* Caullery and Mesnil, 1898, *S. mesnili* Chatton and Dehorne, 1929, *S. caulleryi* Chatton and Villeneuve, 1936, and *S. dogieli* Chatton and Dehorne, 1929. The type species *S. nematoides* was described from the intestine of the polychaete *Scoloplos armiger* (Caullery and Mesnil 1898). Typical features of blastogregarines are epicellular parasitism like gregarines, persistent multinuclearity in trophozoites (unlike gregarines, which are uninuclear), bending motility like archigregarines – the most plesiomorphic gregarine group (Schrével and Desportes 2015; Schrével et al. 2013), and the capacity to produce globular buds, putative stages of game-

togenesis, from their posterior end (Chatton and Dehorne 1929; Chatton and Villeneuve 1936a). This latter feature is unknown from other sporozoans and led to the name "blastogregarines" (i.e., "budding gregarines") (Chatton and Villeneuve 1936a). The life cycle of blastogregarines (Fig. 1) was proposed by Chatton and co-authors relying on evidence from studies on *S. mesnili* and *S. caulleryi* (Chatton and Dehorne 1929; Chatton and Villeneuve 1936a). Although the sexual process was studied incompletely (gamete formation, especially microgametogenesis, and the development of zygote, i.e., sporogony, were not traced), Chatton and Villeneuve suggested that blastogregarines are more similar to coccidians than to gregarines due to the absence of the syzygy and gametocyst (characteristic for gregarines) and their extremely pronounced anisogamy (a coccidian feature) (Chatton and Villeneuve 1936b).

The persistent multinuclearity unusual for sporozoans and the peculiar life cycle (absence of so-called Leuckart's triade: a cyclic sequence of merogony, gamogony, and sporogony, which is characteristic for many sporozoans, e.g., coccidians, haemosporidians, and a part of gregarines (Perkins et al. 2000)) gave rise to discrepant and changeable interpretations of the taxonomic position of blastogregarines following their initial discovery. Different authors considered them as aberrant gregarines (Dogiel 1910), a group incertae sedis within sporozoans (Léger 1909; Léger and Duboscq 1910) or a protistean lineage unrelated to sporozoans at all (Caullery and Mesnil 1899). After more detailed studies on the life cycles of blastogregarines (see above), Chatton and Villeneuve (1936a,b) concluded that the permanent gametogenesis distinguished them from both gregarines and coccidians and suggested considering them as an independent group of the same rank (the order) within Sporozoa (Telosporidia). Grassé (1953a) supposed that blastogregarines should be included in the class Gregarinomorpha. Krylov and Dobrovolskij challenged the assignment of the blastogregarines to the phylum Sporozoa altogether and considered them only as an addendum to that (Krylov and Dobrovolskij 1980). Conversely, de Puytorac et al. (1987) adopted and developed the standpoint of Chatton and co-authors and assigned the blastogregarines as the separate sporozoan class Blastogregarinea along with the classes of gregarines, coccidians, and haemosporidians (de Puytorac et al. 1987). Finally, despite the absence of syzygy, Levine and his followers (Levine 1985; Perkins et al. 2000) assigned the blastogregarines to the order Eugregarinorida

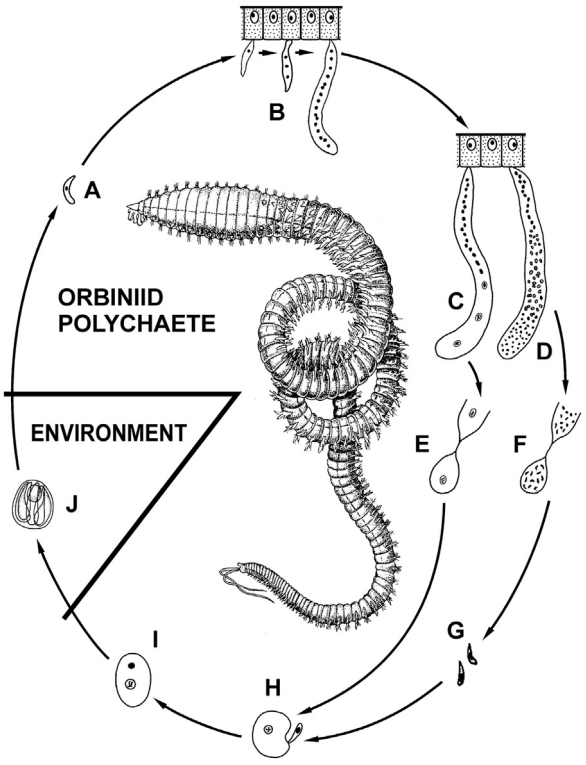

Figure 1. Diagram of the life cycle of blastogregarines according to Chatton and co-authors (Chatton and Dehorne 1929; Chatton and Villeneuve 1936a). (**A**) Young mononuclear vermicular individual similar to sporozoites of coccidians and gregarines. (**B**) Non-differentiated trophozoites attached to the intestinal epithelium of the host; the number of the nuclei increases during trophozoite growth. (**C**, **D**) The epicellular trophozoites develop into the gamonts of two types: macrogamonts (**C**) and microgamonts (**D**); the macrogamonts (female gamonts) have the nuclei arranged in a single row; the size of the nuclei increases towards the rear end of the cell; the microgamonts (male gamonts) have a similar arrangement and size of the nuclei in the anterior third of the cell, after that the distribution of the nuclei, which perform multiple divisions, becomes random and they decrease in size towards the rear end of the cell. (**E–H**) The gamonts attached to the intestinal epithelium produce either numerous uninuclear (**E**) or multinuclear (**F**) globular buds from their posterior ends. Chatton and Villeneuve (1936a) considered this process as gamogony giving rise to macrogametes (**E**, **H**) or multinuclear microgametocytes (**F**), which presumably release small microgametes (**G**). Chatton and colleagues detected stages in the hindgut content that were interpreted as gamete copulation (**H**) and zygotes (**I**). (**J**) Oocysts, found in the feces of the hosts, contain 10-16 free banana-shaped sporozoites (without sporocyst envelopes), and a residual body shifted to one of the oocyst poles. Adapted from (Caullery and Mesnil 1898) (**A**), and (Chatton and Villeneuve 1936a) (**B–J**).

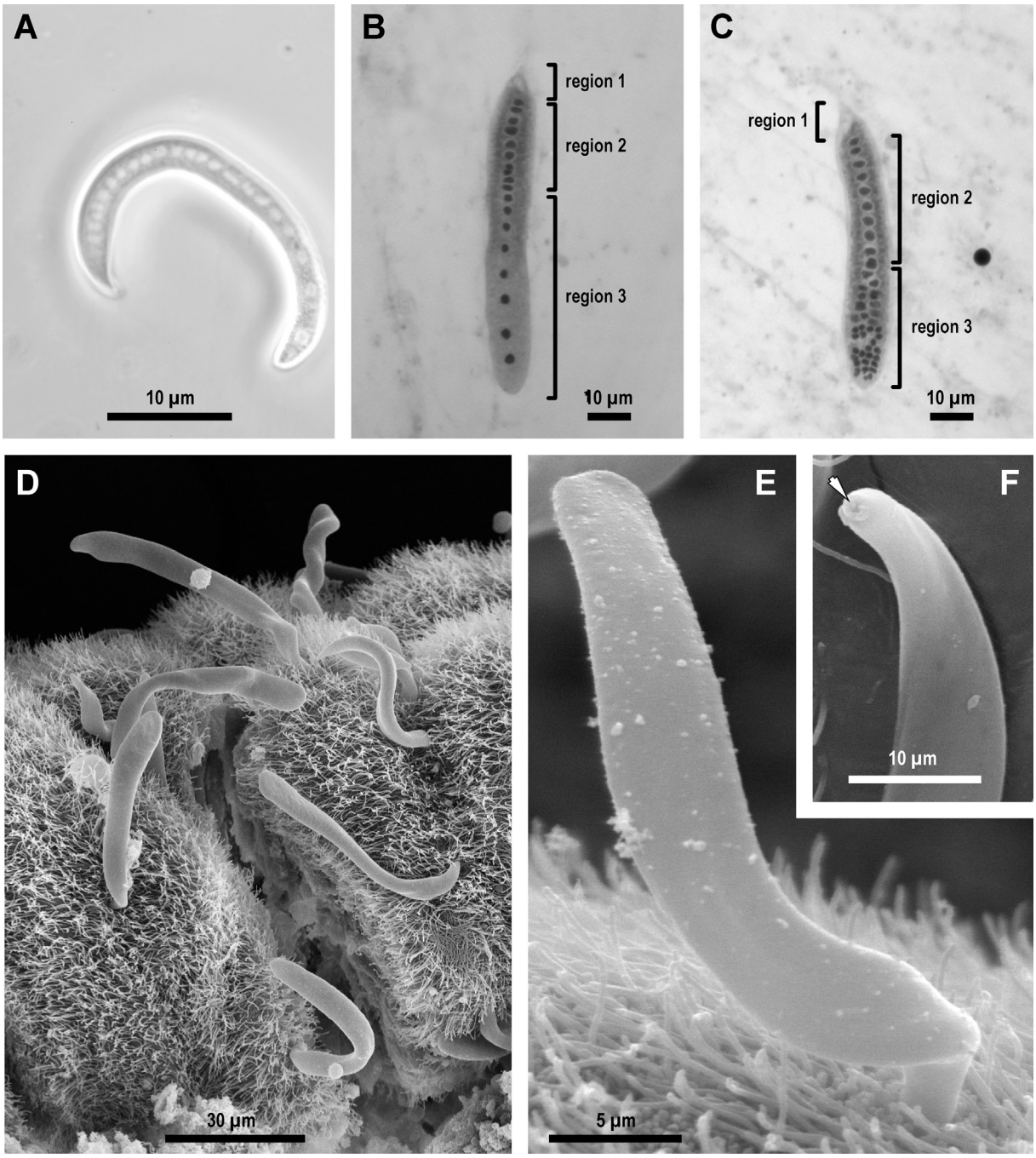

Figure 2. General morphology of the blastogregarine *Siedleckia* cf. *nematoides* ((**A–C**), LM, phase contrast or bright field; (**D–F**), SEM). (**A**) A living macrogamont individual. (**B**) and (**C**) The fixed young macrogamont and microgamont, respectively, stained by Böhmer's hematoxylin, flat views; three regions of the cell are conspicuous: #1 (mucron), #2 ("asexual"), and #3 ("sexual") – see next figure (Fig. 3) and Discussion for further explanations. (**D**) Individuals attached to the intestinal epithelium of the host. (**E**) An individual attached to the intestinal epithelium (under higher magnification) shows the smooth surface of the cell. (**F**) The mucron (arrow) of an individual dislodged from the gut epithelium.

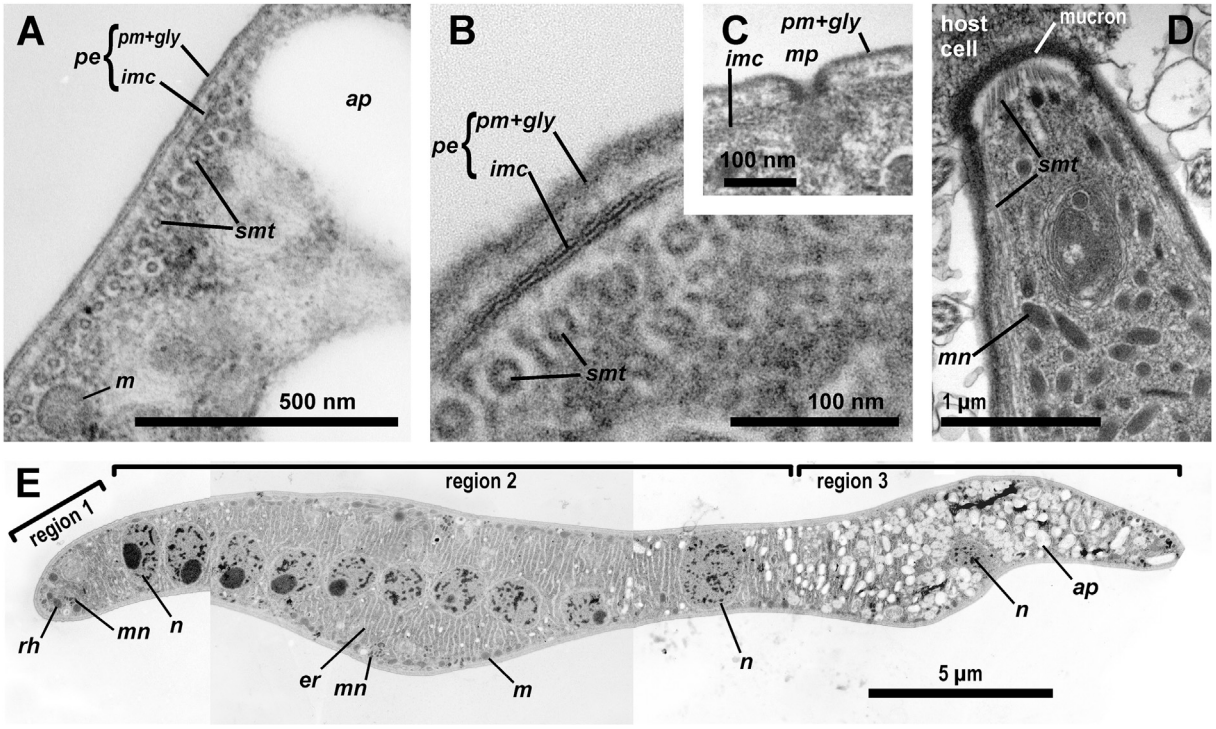

Figure 3. General ultrastructure of the blastogregarine *Siedleckia* cf. *nematoides* (TEM). (**A**, **B**) Cross sections through the cortical region of the cell showing the trimembrane pellicle (*pe*) consisting of the plasma membrane (*pm*) covered by the cell coat (glycocalyx, *gly*) and inner membrane complex (*imc*), longitudinal subpellicular microtubules (*smt*) chiefly arranged in a layer beneath the pellicle; mitochondria (*m*) and the granules of amylopectin (*ap*) are present in the cytoplasm. (**C**) Micropore (*mp*). (**D**) The longitudinal section through a parietal part of the anterior end (region 1–see below) of an individual attached to the host cell showing longitudinal subpellicular microtubules (*smt*) and numerous putative micronemes (*mn*). (**E**) two combined micrographs of the neighbored longitudinal sections of the anterior half of a macrogamont cell showing the subdivision of the cell into three regions: (1) mucronal region with rhoptries (*rh*) and putative micronemes (*mn*), (2) region of the linear arrangement of nuclei (*n*), which is rich in channels of endoplasmic reticulum (*er*), putative micronemes (*mn*), and mitochondria (*m*), and (3) posterior part of the cell (the section covered only its anterior part) rich in amylopectin granules (*ap*); see Figures 4–6 for details.

that was formally explained only by the absence of merogony in their life cycle. This taxonomic scheme has recently been accepted in the WoRMS and NCBI databases. The more recent reviews (e.g., Adl et al. 2012) largely ignored this group likely because of the absence of ultrastructural and molecular phylogenetic evidence that makes their phylogenetic relationships and taxonomic position actually obscure. It should be emphasized that the structure and biology of blastogregarines were not addressed since 1936 (Chatton and Villeneuve 1936a). Thus, the uncertain affiliation of these unusual organisms required efforts to be clarified with the use of modern methods. This work presents the first ultrastructural and molecular phylogenetic evidence from two blastogregarine species, *Siedleckia nematoides* and *Chattonaria mesnili* (formerly *S. mesnili*) gen. n., comb. n., which lead us to redefine the phylogenetic and taxonomic position of the group.

Results

Morphology and Ultrastructure

Siedleckia cf. ***nematoides*** Caullery et Mesnil, 1898. Although the morphology of these blastogregarines collected by us matched the first description of *Siedleckia nematoides* (Caullery and Mesnil 1898) and excellent drawings in a later paper about it (Caullery and Mesnil 1899), we use "cf." (Lat. *confer* – compare with) in the species name because the sampling was performed quite far from the type locality (Gulf of Wimereux, the English Chan-

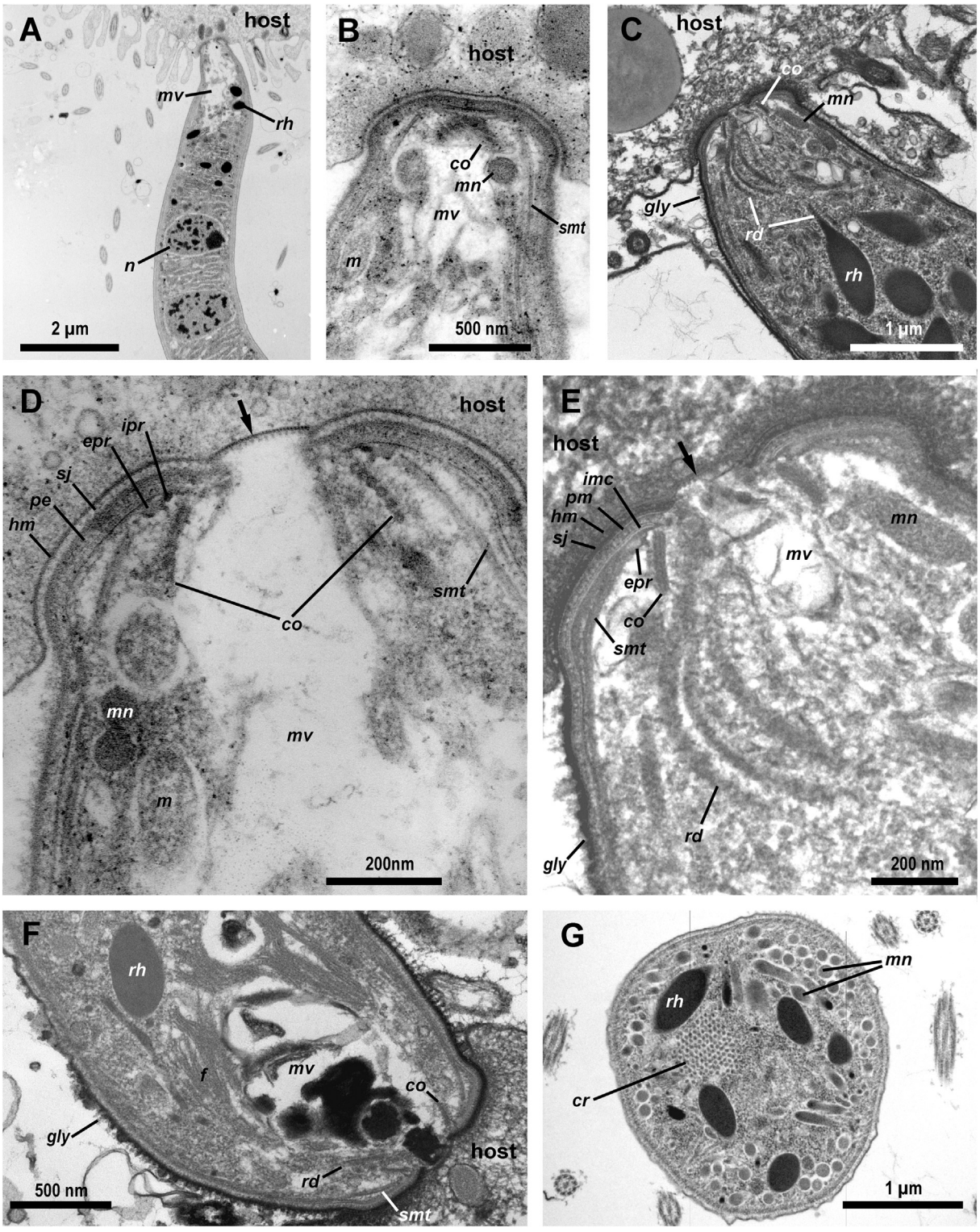

Figure 4. Ultrastructure of the attachment apparatus of the blastogregarine *Siedleckia* cf. *nematoides* (TEM). (**A**) Longitudinal section through the anterior part of a blastogregarine attached to the host intestinal epithelium showing the large mucronal vacuole (*mv*), rhoptries (*rh*), and nuclei (*n*). (**B–F**) Longitudinal sections of the mucron showing the details of its organization: the conoid (*co*), the mucronal vacuole (*mv*), the rhoptries (*rh*) with the ducts (*rd*), external and internal parts of the polar ring (*epr* and *ipr*,

nel, France) and, additionally, due to the possibly existence of cryptic species within this morphospecies (see below). Individuals of *S.* cf. *nematoides* were isolated from the intestine of the polychaete worm *Scoloplos* cf. *armiger* (O.F. Müller, 1776) from two localities in the White Sea, Russia: near Marine Biological Station of Saint Petersburg State University (MBS) and near White Sea Biological Station of Moscow State University (WSBS). All dissected worms (more than 200 individuals) from both localities were infected. The parasites were observed in the midgut (the area behind the stomach) among epithelial cells bearing microvilli and cilia. The intensity of the infection varied from few parasites per host up to 20 cells per 0.01 mm^2 in some loci of the host intestinal epithelium (SEM data on 30 samples). Neither light nor electron microscopy revealed any appreciable differences between individuals of *S.* cf. *nematoides* from the both sampling localities. The cells of *S.* cf. *nematoides* were elongated and flattened with pointed anterior and rounded posterior ends; their smooth surface lacked any grooves and folds (Fig. 2A–E). The cell size varied broadly among individuals: length 5–200 μm (av. 70 μm; mode 60 μm; n = 139), width 3–17 μm (av. 9 μm; mode 8 μm; n = 139) across flattened side, and 1–3 μm (n = 139) across narrow side. Living blastogregarines attached or dislodged from the intestinal epithelium were continuously motile with active bending, twisting, and squirming movements (for details, see: Valigurová et al. 2017).

In female gamonts (=macrogamonts), nuclei were arranged in a row along the cell's length (Fig. 2A, B). They were located closer to each other in the anterior half of the body and appeared compressed and ranged in size from 0.5 × 1.3 up to 0.7 × 2.2 μm (av. 0.9 × 1.3 μm, n = 60 nuclei in 10 individuals). The distance between the nuclei increased and they became a little larger towards the posterior end (from 0.5 × 1.6 up to 1.0 × 2.9 μm; av. 1.1 × 1.7, n = 32, the same 10 individuals). The nuclei in the male gamonts (=microgamonts) were much more numerous (Fig. 2C) with a linear arrangement only in the anterior part of the cell. Like the nuclei of macrogamonts in this region, they were slightly compressed and ranged in size from 0.5 × 1.1 up to 1.8 × 2.2 μm (av. 1.1 × 1.5 μm, n = 56, 10 individuals). In the posterior part of microgamonts, the nuclei were distributed randomly; their shape became irregular and the size decreased (0.5 × 0.7 up to 1.1 × 1.4 μm; av. 0.7 × 0.9, n = 58, the same 10 individuals). The border between these patterns of distribution lay nearly in the middle of the body in smaller (younger) individuals (Fig. 2C) or moved to the anterior third of the body in larger (elder) ones (not shown, see: Caullery and Mesnil 1899). Compared with younger gamonts, the nuclei were more numerous in elder ones, both female and male.

Individuals of *S.* cf. *nematoides* embedded their apical end (mucron) into the brush border of enterocytes bearing microcilia and microvilli (Fig. 2D, E). When dislodged after fixation, some of them, with an intact attachment site, exhibited a small apical pit in its center (Fig. 2F). No additional structures providing attachment, e.g., hooks or other projections, were found.

The tegument of *S.* cf. *nematoides* cells (Fig. 3A, B) was represented by a trimembrane pellicle, 32 nm thick. It consisted of the plasma membrane with a well-developed glycocalyx, and two closely adjacent cytomembranes forming the inner membrane complex, IMC. The internal lamina, an electron-dense layer just beneath the IMC, which is characteristic for gregarines (Schrével et al. 2013) was not detected. A single layer of numerous regularly arranged longitudinal subpellicular microtubules arose from the anterior end and passed along the whole cell (Fig. 3D); each microtubule appeared to be surrounded by an electron-translucent area (Fig. 3A, B). Few additional microtubules were located just beneath this layer (Fig. 3A). Micropores (Fig. 3C) were detected rarely, in the anterior part of the cell. The cell of *S.* cf. *nematoides* is highly polarized and the ultrastructure allowed to define three regions (Fig. 3D, E): (1) the mucron (attachment and feeding apparatus) containing organelles of the apical complex and lacking nuclei, (2) the region of linear arrange-

respectively), longitudinal subpellicular microtubules (*smt*) arising from *epr*, putative micronemes (*mn*), and mitochondria (*m*); the mucron is covered by the pellicle (*pe*) forming a septate cell junction (*sj*) with the host cell; *hm*, plasma membrane of the host cell, *pm*, plasma membrane of the parasite cell, *imc*, inner membrane complex, *gly*, glycocalyx; *arrows* mark the modified part of the host cell surface facing parasite cytostome. Image (**F**) also shows longitudinal thick fibrils (*f*) around the posterior part of the mucronal vacuole. (**G**) Cross section through the anterior part of a blastogregarine cell behind the mucronal vacuole showing a crystalloid structure (*cr*). (**C**, **E**, **F**) fixed in the presence of ruthenium red (see "Methods").

ment of nuclei rich in endoplasmic reticulum (ER), and (3) the posterior half of the body (in full-sized individuals) with significant differences between the macro- and microgamonts in the structure, number, and arrangement of nuclei that will be detailed below.

TEM studies revealed that the attachment apparatus of *S.* cf. *nematoides* is a mucron. It was embedded in the host enterocyte between the microvilli (Fig. 4A) and contained the mucronal vacuole, the conoid, two (internal and external) polar rings, and numerous rhoptries (Fig. 4B–E). The conoid (Fig. 4B–E) had upper and basal diameters of nearly 290 and 400 nm, respectively, and its height was about 130 nm. It was built of coiled microtubules: six microtubules were visible on longitudinal sections (Fig. 4B, D); the anterior three of them were closely adjacent to each other, while the rear three were spaced 6–7 nm apart (Fig. 4D). The polar ring, located slightly higher than the upper opening of the conoid (Fig. 4D, E), gave rise to the longitudinal subpellicular microtubules, i.e., it is their MTOC (the microtubule organization center). The polar ring appeared to be subdivided into two parts of different electron density: external and internal. The external part having moderate electron density was about 40 nm thick with the external diameter about 450 nm. The internal part (Fig. 4D) of high electron density is thinner (~20 nm thick) and narrower (ext. diam ~360 nm, int. diam. ~340 nm) than the external one. The majority of longitudinal sections showed a voluminous mucronal vacuole with a loose fibrous material and a wide duct passing through the conoid and opening outside, i.e. into the space between the parasite and host cells (Fig. 4A–F). Several large rhoptries were distributed around and behind the mucronal vacuole; they formed ducts passing through the conoid and, apparently, opened outside the cell (Fig. 4C, E). Few putative micronemes and mitochondria were detected in the parietal area of the anterior region of the mucron (Fig. 4B–E). The number of the putative micronemes increased in the region behind the mucronal vacuole where they had a regular distribution on the periphery of cytoplasm (Figs 3D, 4G). The mucron was covered by the trimembrane pellicle excepting the region against the conoid with the wide inlet opening (diam. ~130 nm) of the mucronal vacuole: we consider it to be a cytostome-cytopharyngeal complex performing myzocytosis (Fig. 4D, E). The cytostome was opened into a gap (~20 nm) between the parasite and host cell plasma membranes, which had the appearance of the septate cell junction; the "septa" were putatively formed by both parasite and host cell coats (Fig. 4D, E). The region of host plasma membrane facing the parasite cytostome was of higher electron density than the rest of the membrane and had uniformly spaced electron-dense structures appeared as bold dots on the external surface of the host cell (Fig. 4D, E); it might be a perforated or modified host cell coat. No other significant modifications of the host cell were detected. Some additional structures were observed in the mucron and the region just behind it: thick fibrils around the posterior part of the mucronal vacuole, and a crystalloid structure (Fig. 4G).

The main feature of the anterior half of the cell behind the mucron (region 2) is the linear arrangement of nuclei (Fig. 3E). Another conspicuous characteristic is the abundance of the channels or cisterns of the endoplasmic reticulum (ER), arranged uniformly in the cytoplasm, chiefly perpendicularly to the longitudinal cell axis (Fig. 5). Occasionally, they were connected to the nuclear envelopes (Fig. 5A). In the subcortical layer of the cytoplasm, mitochondria and putative micronemes were numerous (Figs 3E, 5); the latter were concentrated in the lateral areas (Fig. 5A). Golgi apparatus, few small granules of amylopectin (the storage carbohydrate), and multimembrane structures were also observed in this cell region (Fig. 5).

In the macrogamont cells, the number and size of the amylopectin granules dramatically increased from the middle of the cell (region 2) towards its rear end (region 3) (Fig. 3E). In the region 3 of the cell, the ER was displaced with these granules (Figs 3E, 6A). In addition, rare large electron-dense globules (not observed in the anterior half of the cell) were present here (Fig. 6A). All nuclei in the macrogamont cells had similar structure: they contained small clods of heterochromatin and a single nucleolus, however, the nuclei in the posterior region were slightly larger than those in the region 2 of the cell: about 1-2 $\times$ 2 μm and 1.2 $\times$ 1.7 μm, respectively (Figs 3E, 6A).

Unlike macrogamonts, the structure of nuclei in the microgamont cells changed from the anterior to the posterior end of the body, with a gradual increase in chromatin condensation (Fig. 6B, C). In the middle of the cell (region 2), the nuclei were completely filled by highly condensed chromatin (Fig. 6B). Raikov called such nuclei "of spermal type" in his classification of protist nuclei (Raikov 1982). From the border between regions 2 and 3 and further towards the rear, the linear arrangement of the nuclei became disordered and the dividing nuclei were repeatedly observed; some of them were equipped with kinetosomes (Fig. 6C–E).

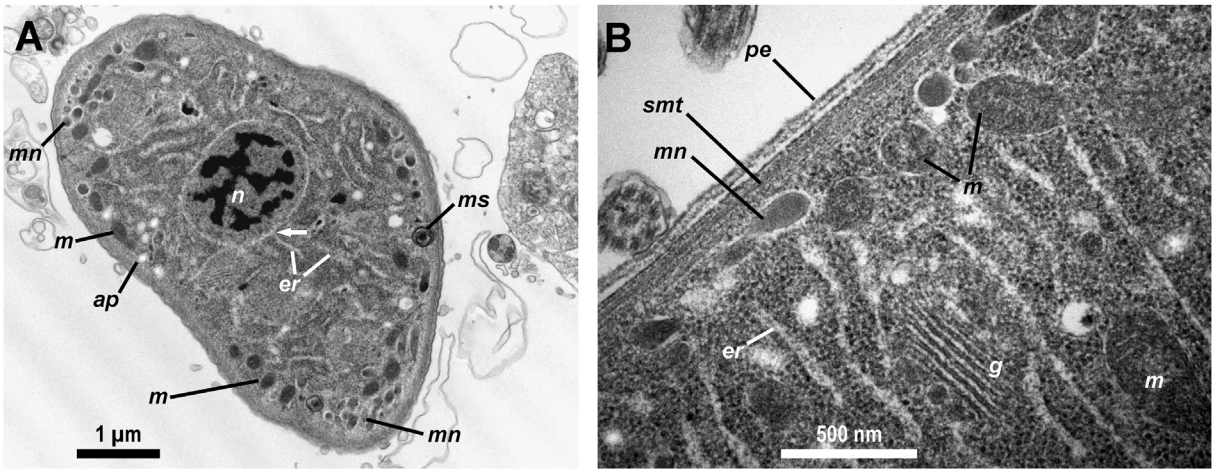

Figure 5. Cytoplasmic organelles of the blastogregarine *Siedleckia* cf. *nematoides* (TEM). (**A**) Cross section through the region 2 of the cell (linearly arranged nuclei) showing putative micronemes (*mn*) in the lateral regions of the cell and a connection of the endoplasmic reticulum (*er*) with the nuclear envelope (arrow). (**B**) Fragment of the longitudinal section of the same region as in (A) showing Golgi apparatus (*g*), abundant channels of the endoplasmic reticulum (*er*), numerous mitochondria (*m*), and putative micronemes (*mn*). Other abbreviations: *ms*, the multimembrane structure; *n*, nucleus; *pe*, pellicle; *ap*, amylopectin granules; *smt*, longitudinal subpellicular microtubules.

Electron-translucent areas within the dividing nuclei contained microtubules, probably the elements of a mitotic spindle (Fig. 6D, E). The connection of these microtubules with the kinetosome or any other possible MTOC was not observed. The nuclear divisions in the region 3 of the microgamont cells obviously correspond to progamic mitoses resulting in the production of microgametes based on the the appearance of two adjacent kinetosomes (Fig. 6D, E). The cytoplasm of the posterior region in the microgamont cells had a completely different structure than that of the macrogamont cells due to the presence of the ER channels and only few small amylopectin granules (Fig. 6D, E).

Chattonaria* (*Syn. Siedleckia*) *mesnili* (*Chatton et Dehorne, 1929) gen. n., comb. n. Individuals of *Chattonaria mesnili* were isolated from the intestine of the polychaete worms *Orbinia* (Syn. Aricia) *latreillii* (Audouin et H. Milne Edwards, 1833) (Orbiniidae) collected on littoral zone of English Channel, France (see "Methods" for details). We managed to sample only 12 individuals of the host species *Orbinia latreillii*, four of them were free of parasites and eight were infected. The parasites were found in the stomach – the dilated part of the intestine situated immediately after the esophagus and covered by glandular cells lacking cilia. The intensity of infection varied from few to tens of parasites (30–40) per host (the latter was observed only in two worms). As a direct consequence of difficulties to sample hosts with a high prevalence of the blastogregarine parasites, the number of *C. mesnili* cells analyzed under SEM, and TEM was significantly lower than in *S.* cf. *nematoides*. LM studies were not performed especially as the collected cells fully fit the first description of *Siedleckia mesnili* and its drawings of excellent quality (Chatton and Dehorne 1929). The collected cells were elongated (48.8×7.6 to 220×13 µm; av. 97.4×9.1 µm; n = 8) and cylindric with a roundly pointed posterior end. Their tegument formed longitudinal folds (Fig. 7A–E). These originated behind the mucron, where pairs of adjacent folds shared a common origin (Fig. 7D), and ran towards the posterior end of the cell, where they merged into a smooth terminal region (Fig. 7E). The number of the folds was 28 and 34 on the cross-sections of two different individuals. The anterior ends of the parasites were embedded in the cells of the host stomach (Fig. 7A). One of the individuals, artificially dislodged during mounting of the SEM preparation, exhibited the anterior end covered with a remnant of the host tissue, therefore we were not able to observe the superficial structure and the shape of the attachment apparatus (Fig. 7B, D), however, the first description suggested it equipped with hooks. In contrast to *S.* cf. *nematoides*, the living individuals of *C. mesnili* observed under a stereomicroscope immediately after the host dissection showed only weak motility by slow and intermittent bending movements.

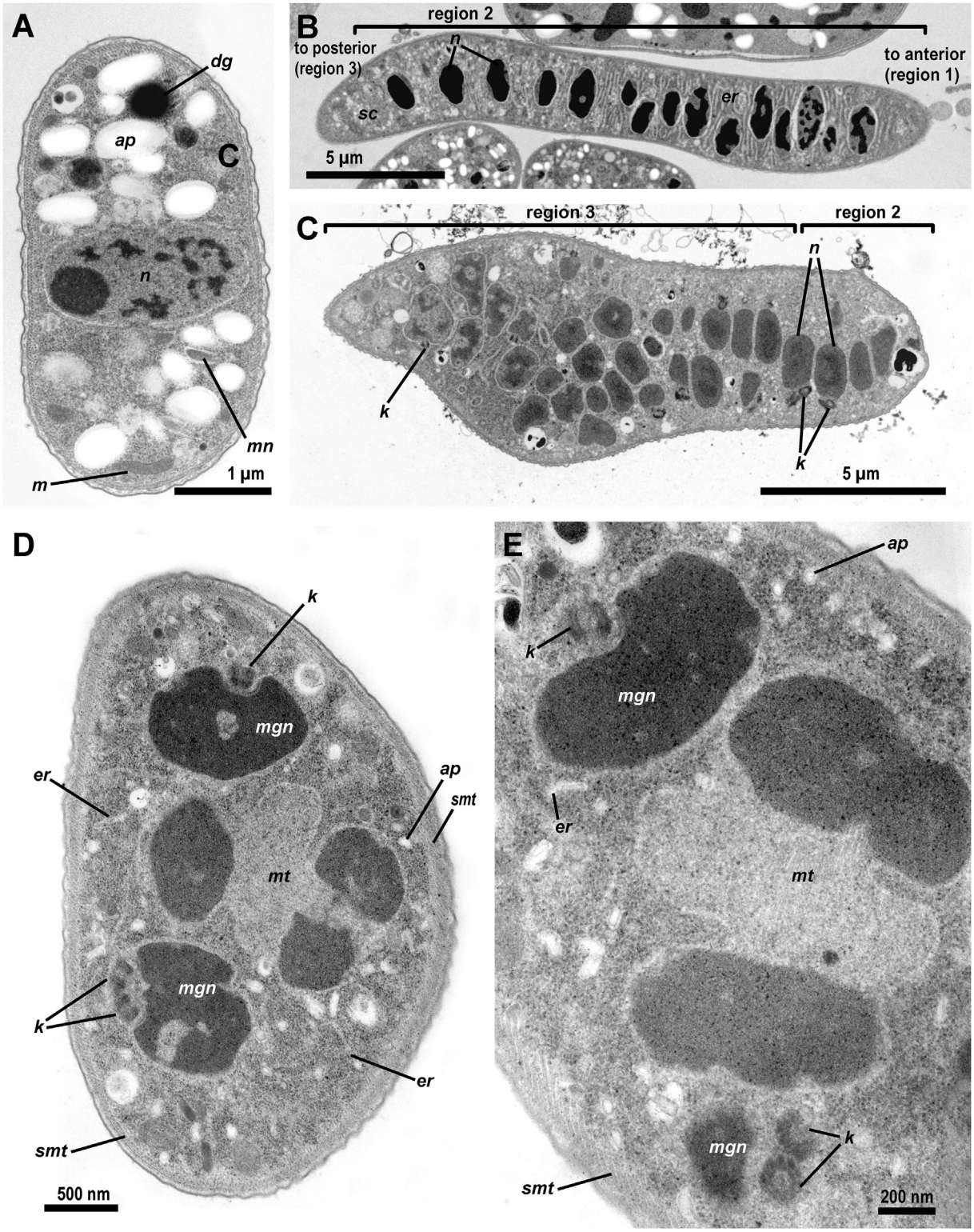

Figure 6. Nuclear apparatus of the blastogregarine *Siedleckia* cf. *nematoides* (TEM). (**A**) The cross section through the rear part (region 3) of a macrogamont cell showing the abundance of amylopectin granules of large size (*ap*), a mitochondrion (*m*), putative micronemes (*mn*), an electron-dense globule (*dg*), and a nucleus (*n*) containing heterochromatin and a nucleolus. (**B**) The longitudinal section of a microgamont cell in the

The cells of *C. mesnili* were covered by the trimembrane pellicle about 50 nm thick and organized in longitudinal folds with flattened tops (Fig. 7F, G). The size of the folds was about 1.1 μm high and 0.9 μm wide at their bases. The height was more and the width was less in the anterior part of the cell: about 2 and 0.3 μm at the bases, respectively, so the shape varied depending on the section site (compare Fig. 7F and G). Just beneath the pellicle, numerous longitudinal subpellicular microtubules were observed, with a regular distribution and arrangement: two layers in the tops of the folds and a single layer on their lateral sides and between them (Fig. 7G). Although no typical micropores were observed, micropore-like structures interrupting the IMC and the layer of subpellicular microtubules and connected to multimembrane vesicles were present (Fig. 7G, compare with Fig. 5A). Similarly to *S.* cf. *nematoides*, the cell of *C. mesnili* can be subdivided into three regions: (1) the mucronal region, (2) the region of the linearly arranged nuclei, and (3) the posterior region with developing gametic nuclei.

TEM studies revealed that the attachment apparatus of *C. mesnili* is a strongly modified mucron lacking the conoid and anchored in the host cell with peripheral bulges (several or the only circular one) formed by large alveoli between the cytomembranes of the IMC (Figs 7B, E; 8A–D, G). One observation suggested that a hook-like cytoplasmic projection jutted into the alveolus (Fig. 8A, C). The flat top of the mucron was covered by the pellicle of varying thickness (~14 to 27 nm) with a loose layer of fibrils just beneath it. In this region, the middle and inner membranes of the IMC terminated around an external opening (cytostome) of the mucronal vacuole. The diameter of the cytostome was about 110 nm (Fig. 8E). Similarly to *S.* cf. *nematoides*, a gap of varying width (~20 to 45 nm) was present between the parasite pellicle and the host cell membrane, but that was not a septate cell junction because of the absence of "septa". The host plasma membrane had an increased electron density in front of the cytostome (Fig. 8D–F**)**. The frontal region of the mucron cytoplasm was free of organelles, with an exception of the mucronal vacuole connected to the cytostome by a wide duct (Fig. 8D, E). Near the IMC terminus, a structure similar to an apical polar ring was observed (Fig. 8E, F). This putative polar ring (~27 nm thick, ext. diam. ~240 nm) was not subdivided into any parts, as it was observed in *S.* cf. *nematoides*, and no microtubule contacting with it were detected, even though they were abundant within the mucron. The microtubules arose immediately from the fibrillar matter lying beneath the pellicle in the frontal region of the mucron. Numerous longitudinal microtubules were located in the cytoplasm behind the mucronal vacuole (Fig. 8D, E). Microneme-like bodies were detected in the parietal region of the mucron (Fig. 8D), but no obvious rhoptries or rhoptry ducts were observed. However, large electron-dense globules (~300 nm in diameter) without ducts were present in the region behind the mucron and around the first nucleus (Figs 8A, B; 9A).

The first non-differentiated nuclei of both macro- and microgamonts cells were slightly ellipsoid in shape (up to ~1.5 × 1 μm) and contained 1 nucleolus (Figs 8A–B; 9A–B). The channels of the ER, dense bodies (likely micronemes), and putative mitochondria were also present.

The region of linearly arranged nuclei (region 2) was studied only in the macrogamonts. The nuclei (up to ~2 × 1.5 μm) contained one nucleolus and heterochromatin that tended to congregate in a single lump (Fig. 9C). Other observed organelles include the small microneme-like bodies (Fig. 9C, D), few small amylopectin granules, putative mitochondria, and well developed ER; however, unlike *S.* cf. *nematoides*, the ER did not exhibit the regular arrangement (Fig. 9C).

The posterior end (region 3) of the macrogamont cells showed nuclei (up to ~1.7 × 1.2 μm) with the circular arrangement of the heterochromatin and excentric nucleolus. The cytoplasm appeared vacuolated and contained numerous

middle of the body (posterior part of region 2) and (**C**) the diagonal section of a microgamont cell through the border between regions 2 and 3: abundant nuclei (*n*) with the highly condensed chromatin are arranged in the raw in region 2; they acquire kinetosomes (*k*) near the border between regions 2 and 3 and then become arranged randomly; (**C**) fixation in the presence of ruthenium red. (**D**, **E**) Cross sections through the rear part of a microgamont cell (region 3) showing the channels of endoplasmic reticulum (*er*), the small and rare granules of amylopectin (*ap*), a putative progamic mitosis, and the nuclei of future microgametes (*mgn*) associated with the kinetosomes (*k*). Note microtubules, probably of the mitotic spindle: (*mt*) and compare with the subpellicular microtubules (*smt*).

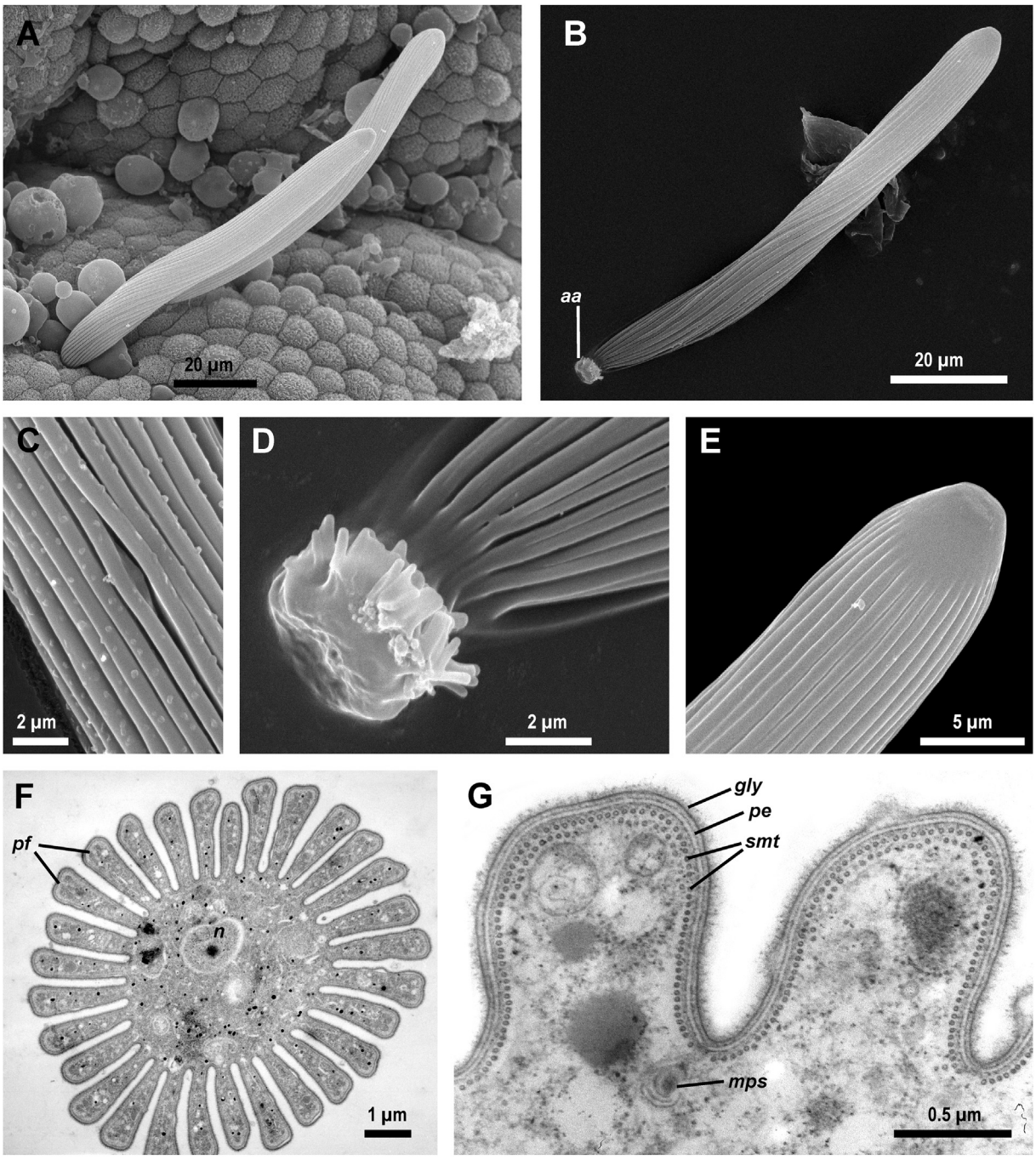

Figure 7. General morphology and cortex organization of the blastogregarine *Chattonaria mesnili* ((**A**–**E**) SEM; (**F**, **G**) TEM, cross sections). (**A**) Two individuals attached to the stomach epithelium of the host. (**B**) An individual artificially dislodged from the epithelium during mounting of the SEM preparation exhibiting the attachment apparatus (*aa*) embedded in the fragment of the intestinal lining. (**C**–**E**) Details of (**B**) under higher magnifications: surface with longitudinal pellicular folds (**C**), the attachment apparatus (*aa*) covered by the remnant of the host tissue (**D**), and the smooth posterior end (**E**). (**F**) Cross section of an individual through anterior region of the cell showing transversally cut longitudinal pellicular folds (*pf*) and a nucleus (*n*) with a single nucleolus. (**G**) A fragment of another cross section under higher magnification showing trimembrane pellicle (*pe*) coated by glycocalyx (*gly*), longitudinal subpellicular microtubules (*smt*) located just beneath it, and a micropore-like structure (*mps*).

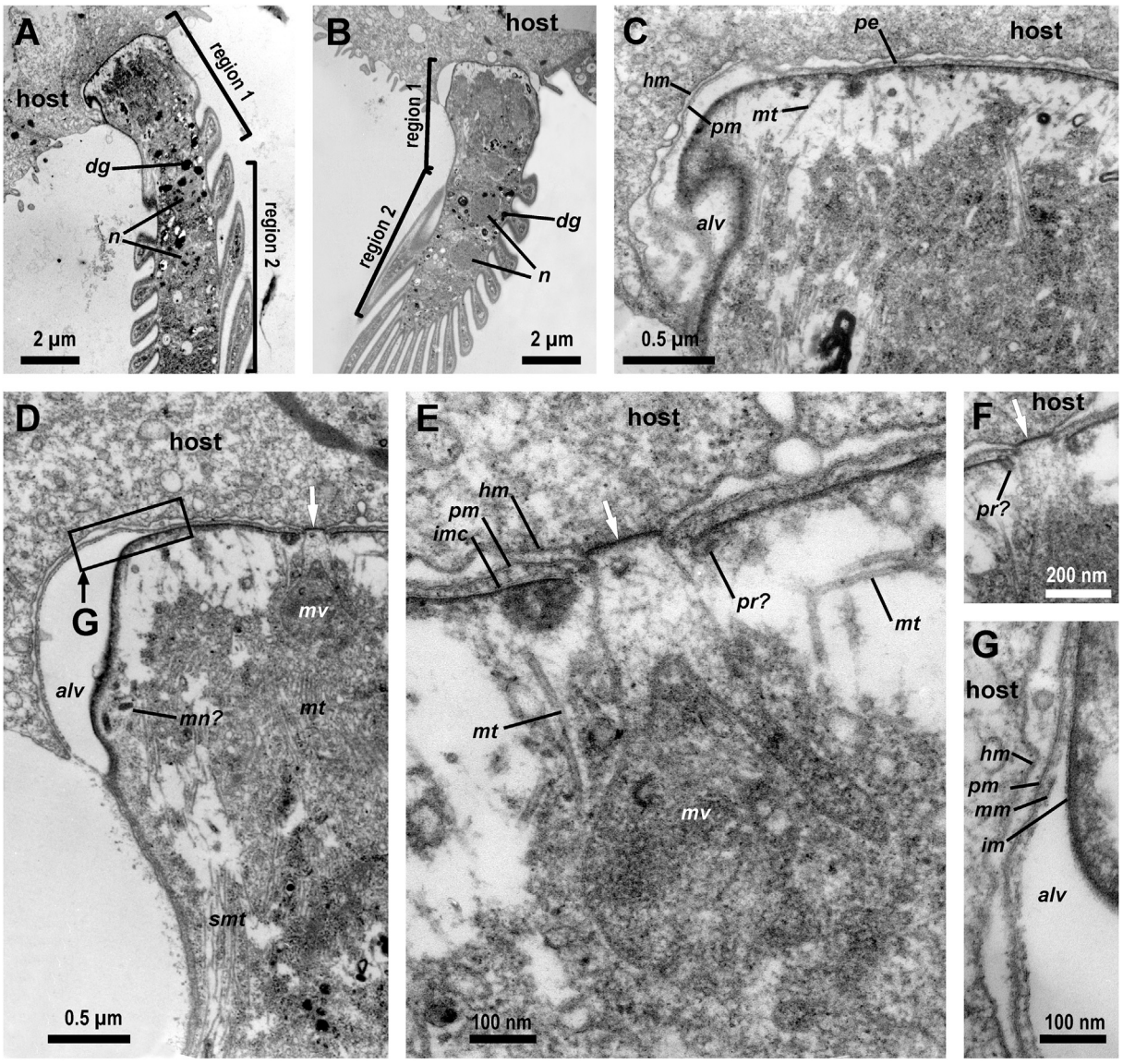

Figure 8. Attachment apparatus (mucron) of the blastogregarine *Chattonaria mesnili* (TEM). (**A–B**) Longitudinal sections of anterior parts of two individuals attached to the host cells: a microgamont (**A**) and a macrogamont (**B**) showing nuclei (*n*) and dense globules (*dg*) in the cytoplasm; two marked regions are corresponding those of *S*. cf. *nematoides* (see Fig. 3). (**C**) Longitudinal section of the same individual that in (A) showing a large alveolus (*alv*) with a protrusion of the cytoplasm and microtubules (*mt*) arising from the pellicle (*pe*) of the mucron; *hm* and *pm* are host and parasite plasma membranes, respectively. (**D–F**) Longitudinal sections of the mucron and its parts of the same individual as in (B) showing myzocytosis through the cytostome facing the electron-dense region of the host cell plasma membrane (white arrow), mucronal vacuole (*mv*), putative polar ring (*pr?*) closely adjacent to endings of the IMC (*imc*), subpellicular microtubules (*smt*) without any visible MTOC, microtubules (*mt*) arising from the frontal zone of the mucron, microneme-like bodies (*mn?*), the cell junction, which is a non-septate gap between parasite and host plasma membranes (*pm* and *hm*, respectively). (**G**) A detail of (D) showing the structure of the large alveolus (*alv*) formed as space between the middle (*mm*) and inner (*im*) membranes of the pellicle; *hm* and *pm* are the plasma membranes of the host and parasite cells, respectively.

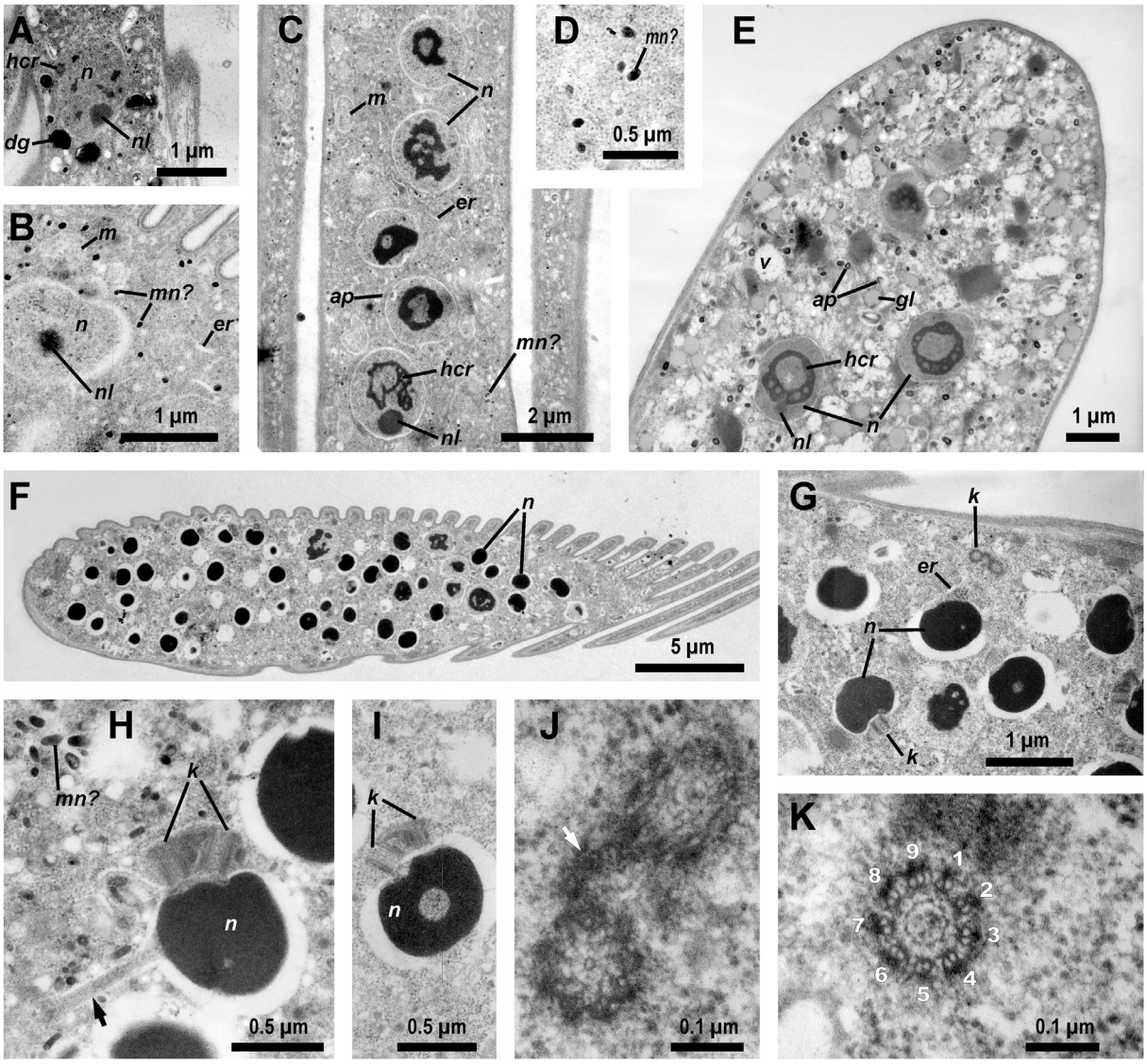

Figure 9. Nuclear apparatus and cytoplasm of the blastogregarine *Chattonaria mesnili* (TEM). (**A**) The first nucleus of a microgamont (the same cell as in Fig. 8A) containing heterochromatin (*hcr*) and a single nucleolus (*nl*) and surrounded by large dense globules (*dg*). (**B**) Fragment of a cross section through the anterior part of a macrogamont (the same cell as in Fig. 7F) showing a nucleus with a single nucleolus (*nl*), but lacking heterochromatin; the channels of the endoplasmic reticulum (*er*), microneme-like bodies (*mn?*), and a putative mitochondrion (*m*) are visible. (**C**) Longitudinal section of the middle part of a macrogamont cell (region 2, corresponding that of *S.* cf. *nematoides*) showing nuclei with the large lumps of the heterochromatin (*hcr*) and a single nucleolus (*nl*, visible in the lowest nucleus), the channels of the endoplasmic reticulum (*er*), putative mitochondria (*m*), rare small granules of the amylopectin (*ap*), and microneme-like bodies (*mn?*). (**D**) Fragment of the cytoplasm (the same region as in (C)) showing microneme-like bodies (*mn?*) under a higher magnification. (**E**) Longitudinal section of the posterior end of a macrogamont (region 3, corresponding to that of *S.* cf. *nematoides*) showing nuclei with the large lumps of the heterochromatin (*hcr*) and weakly developed nucleoli (*nl*, visible in the left lower nucleus); the cytoplasm is vacuolated (*v*, vacuoles) and contains numerous globules (*gl*), putatively of protein, and grains of amylopectin (*ap*). (**F–I**) Diagonal sections of the posterior parts of microgamonts (region 3) under different magnifications showing numerous randomly distributed male gametes' nuclei (*n*) associated with two kinetosomes (*k*) and connected to the main cytoplasm with a stalk (black arrow); the cytoplasm contains numerous microneme-like bodies (*mn?*, in (H)). (**J**) cross-section through two kinetosomes connected with an electron-dense link (white arrow). (**K**) cross section of the top of a kinetosome (the transitive zone to the future flagellum) showing 9 groups (doublets) of microtubules.

globules (putatively proteins), and amylopectin granules not abundant in this region (Fig. 9E). The posterior end of the microgamont cells contained numerous spherical (~0.6 μm in diameter) nuclei of "spermal" type according to the classification by Raikov (1982) with highly condensed chromatin in the whole volume (Fig. 9F – I). Each nucleus was encircled by an electron-translucent zone; some with a stalk connected them to the main cytoplasm (Fig. 9H). Most nuclei were associated with two kinetosomes containing nine peripheral groups of microtubules, apparently triplets or doublets depending on the kinetosome region; the kinetosomes were connected to each other by an electron-dense link (Fig. 9J, K). The cytoplasm appeared vacuolated, with abundant microneme-like bodies (Fig. 9H); the amylopectin granules and putative protein globules were not detected. No mitochondria were observed in the posterior regions of both macrogamont and microgamont cells.

Molecular Phylogenetic Analyses

For *S.* cf. *nematoides*, the contiguous sequence of the near-completed ribosomal operon (SSU rDNA + ITS1 + 5.8S rDNA + ITS2 + LSU rDNA) was obtained from the WSBS sample, whereas only a partial sequence of SSU rDNA was obtained from the MBS sample. For the sample of *C. mesnili*, the obtained contiguous sequence covered near-complete gene of SSU rRNA, ITS1, 5.8S rDNA, ITS2, and a large part (~2,000 bp) of LSU rDNA (Table 1). All these sequences were involved in phylogenetic analyses with the use of Bayesian inference (BI) and Maximum likelihood (ML) methods (see "Methods" for details).

Analyses of 18S (SSU) rDNA. Both Bayesian inference and Maximum likelihood (ML) analyses resulted in almost identical tree topologies with some differences in the branching within the coccidia + hematozoa clade (not shown). The Bayesian tree appeared more accurate than the ML one: in the ML tree *Plasmodium* spp. grouped not with piroplasms, but with adeleid coccidians, although with low support (BP = 38%), i.e. hematozoans were split up. We consider this an artifact, which is absent in the Bayesian tree. This point does not affect the position of blastogregarines and neighboring branches. The higher accuracy of Bayesian inference than ML bootstrap analysis was also revealed previously (Alfaro et al. 2003). Overall the newly obtained phylogenies matched molecular phylogenetic evidence from alveolates and apicomplexans published recently (e.g., Cavalier-Smith 2014; Janouškovec et al., 2015; Lepelletier et al. 2014; Rueckert and Horák 2017; Schrével et al. 2016). The Bayesian tree inferred from the dataset of 110 taxa and 1,550 sites (Fig. 10) showed the monophyly of major alveolate groups, although with moderate or low statistical support. The backbone of the apicomplexan region in the newly obtained tree was poorly resolved by both Bayesian and ML analyses. The three obtained blastogregarine sequences together with environmental sequence D3P05D06 formed a clade with full PP (posterior probabilities in Bayesian analysis) and high BP (bootstrap percentage in ML analysis) supports (1.0 and 90%, respectively). This robust blastogregarine clade was located between two archigregarine lineages, but all node supports in this region of the tree backbone were extremely low (Fig. 10). The archigregarine split had been already recovered before, also with very weak supports (Rueckert et al. 2015; Rueckert and Horák 2017; Schrével et al. 2016; Wakeman et al. 2014; Wakeman and Horiguchi 2017; Wakeman and Leander 2013), i.e. this is not an effect of the addition of blastogregarines to the taxon sampling. SSU rDNA identities between the two *S.* cf. *nematoides* samples and the environmental sequence D3P05D06 were at about 90% (MBS vs. D3P05D06 = 90%, WSBS vs. D3P05D06 = 92.1%, WSBS vs. MBS = 93.7%), whereas those between *C. mesnili* and *S.* cf. *nematoides* were lower, at 82.8%–83.9% (see Supplementary Material Table S1 for details).

Analyses of 28S (LSU) rDNA and the ribosomal DNA operon. All phylogenies based on these phylogenetic markers resulted in identical topologies both in the Bayesian (Fig. 11) and ML (not shown) analyses. Overall, they recovered the major alveolate clades that agreed the phylogenies inferred from SSU rDNA – both already published (see above) and newly obtained – but with the higher resolution of all-alveolate and myzozoan deep branching than in SSU rDNA trees.

In the LSU rDNA-alone-based phylogeny (Fig. 11A), the monophyletic apicomplexan clade comprised the moderately supported chrompodellid lineage and sporozoans; the latter were subdivided into the clades of firmly supported coccidiomorphs (coccidians + hematozoans) and moderately supported by BP cryptosporidians + gregarines. All presented (available) gregarine sequences formed a monophyletic clade, although the BP support was only moderate (PP = 1.0, BP = 84%). Similar val-

ues of BP supports were also obtained for other nodes in the backbone of this clade. The monophyly of eugregarines was broken due to the archigregarine *Selenidium* sp. In contrast to the SSU rDNA phylogenies, the blastogregarine LSU rDNA sequences showed no affinity to gregarines, but formed a sister branch to the coccidiomorph clade, although with rather low PP and BP supports (0.67 and 52%, respectively).

Compared with the LSU rDNA, phylogenies using the near complete ribosomal DNA operons (concatenated SSU, 5.8S, and LSU rDNAs) showed higher BP supports for the dinozoans and for the sporozoans (Fig. 11B). In contrast, BP supports for the cryptosporidians + gregarines clade and its internal branching decreased. The sistership of the blastogregarines and coccidiomorphs was also recovered, although with lower support (PP = 0.50, BP = 37%).

Testing alternative topologies. The alternative topologies of phylogenetic trees were analyzed with the use of the set of six widespread tests (see "Methods" for details). Among 12 alternative SSU rDNA phylogenies (Supplementary Material Fig. S1), six were found to reject by no test (Fig. 12A); four of them represented the blastogregarines as a member of the clade cryptosporidians + gregarines and two as a sister group either to this clade or to the sporozoans as a whole. However, approximately unbiased test and majority of others did not reject any alternative topology including the direct association of the blastogregarines with the coccidiomorph clade (see Supplementary Material Table S2 and Fig. S1, topologies #7 and 10). However, the boostrap probability rejected this location (topologies #7 and 10 in the Supplementary Material Fig. S1), even though it was the best in the LSU rDNA and the ribosomal operon phylogenies (Fig. 11, the reference topologies #0 and alternative topologies #1 in Fig. 12B and C). In contrast, among LSU rDNA and ribosomal operon phylogenies, all tests rejected any position of the blastogregarines within the cryptosporidian + gregarine clade, as chiefly preferred in SSU rDNA phylogenies (Supplementary Material Table S2; Fig. 12B, C). However, no test rejected the blastogregarines as the sister group to all other sporozoans. In summary, the blastogregarines as the earliest branch of the sporozoans was the only case permitted by all tests in all three genetic markers examined (i.e., SSU rDNA, LSU rDNA, and ribosomal operon phylogenies).

Discussion

The general morphology and ultrastructure of blastogregarines represent a fanciful combination of the features characteristic to different far-related taxa of sporozoans (Fig. 13). This is congruent with the uncertain position of blastogregarines within the sporozoans provided by the conflicting SSU rDNA and LSU rDNA ribosomal operon molecular phylogenies. On the one hand, blastogregarines share many ultrastructural features with archigregarines, the most plesiomorphic group of the sporozoans known to date (Schrével 1971b; Schrével and Desportes 2015; Schrével et al. 2013) – that agrees with SSU rDNA-based phylogenies placing these organisms in the close neighborhood to each other, although with low supports. First, both blastogregarines and archigregarines possess longitudinally folded or smooth pellicle – in archigregarines, the latter is rare, but sometimes exists (Simdyanov 1992) – and longitudinal subpellicular microtubules arranged in layer(s) just beneath it (Schrével 1971a,b; Simdyanov and Kuvardina 2007). Second, the mucron and apical complex in both these groups does not disappear in the early developmental stages as in majority of sporozoans, but persists over a long period of time: during the larger part of their life cycle indeed. The trophic stages of both blastogregarines and archigregarines attach to host cells with the mucron that contains the mucronal vacuole and well-developed components of the apical complex (at least in *S.* cf. *nematoides* among blastogregarines) and performs myzocytotic feeding (Schrével 1968, 1971b; Simdyanov and Kuvardina 2007). In blastogregarines, this mucronal complex (the apical complex and mucronal vacuole) remains active (myzocytosis) during the trophozoite lifespan. Unlike blastogregarines, archigregarines have non-feeding mature gamonts (syzygy stage), but the conoid and rhoptries persist in them until starting progamic mitoses at least (Schrével et al. 2013; Simdyanov and Kuvardina 2007). Despite generally plesiomorphic body plan, the studied blastogregarines exhibit modifications of the cortex and mucron, which can be considered autapomorphies, and they show a mosaic distribution. Thus, the folded pellicle characteristic for both *C. mesnili* and many *Selenidium* spp. appears to be a plesiomorphic trait, but the major modification of its mucron (loss of conoid and rhoptries) is a distinct apomorphy. On the contrary, *S.* cf. *nematoides*, has a plesiomorphic mucron with the complete apical complex; however, its smooth pellicle appears rather an apomorphy. The more

Table 1. The main characteristics of the obtained blastogregarine sequences: the source and total length of assembled contiguous sequences, the length of overlapping PCR-amplified fragments used for their creation, and PCR primers used for the amplification of the fragments.

Sources and total lengths of assembled sequences	Amplified fragments[a]	Fragment length	PCR primers: forward (F) and reverse (R); annealing temperature used in the PCRs
Siedleckia cf. *nematoides* from MBS (1,645 bp) MH061197	SSU rDNA (part)	1,645 bp	(F) 5′-GTATCTGGTTGAT CCTGCCAGT-3′ (R) 5′-GCGACGGGCGGTGTGTAC-3′ t° = 48 °C
Siedleckia cf. *nematoides* from WSBS (5,617 bp) MH061198	(I) SSU rDNA (part)	1,765 bp	(F) 5′-GTATCTGGTTGAT CCTGCCAGT-3′ (R) 5′-GAATGATCCWTC MGCAGGTTCACCTAC-3′ t° = 48 °C
	(II) SSU rDNA (part), ITS1, 5.8S rDNA, ITS2, LSU rDNA (part)	2,004 bp	(F) 5′-GCATGGCCGTTCT TAGTTGGTGG-3′ (R) 5′-CCTTGGTCCGTGTTTCAAGAC-3′ t° = 48 °C
	(III) LSU rDNA (part)	1,021 bp	(F) 5′-ACCCGCTGAAYTT AAGCATAT-3′ (R) 5′-GCTATCCTGAGGG AAACTTCGG-3′ t° = 53 °C
	(IV) LSU rDNA (part)	1,549 bp	(F) 5′-GTCTTGAAACACG GACCAAGG-3′ (R) 5′-CAGAGCAGTGGGC AGAAATC-3′ t° = 53 °C

Table 1 (*Continued*)

Sources and total lengths of assembled sequences	Amplified fragments[a]	Fragment length	PCR primers: forward (F) and reverse (R); annealing temperature used in the PCRs
	(V) LSU rDNA (part)	1,001 bp	(F) 5′-GTAACTTCGGGAW AAGGATTGG CT-3′ (R) 5′-GTCTAAACCCAGC TCACGTTCC CT-3′ t° = 53 °C
Chattonaria mesnili (4,560 bp) MH061199	(VI) SSU rDNA (part)	1,782 bp	(F) 5′-GTATCTGGTTGAT CCTGCCAGT-3′ (R) 5′-GATCCTTCTGCAG GTTCACCTAC-3′ t° = 48 °C
	(VII) SSU rDNA (part), ITS1, 5.8S rDNA, ITS2, LSU rDNA (part)	∼1,600 bp	(F) 5′-GTCCCTGCCCTTT GTACACACCGCCCG-3′ (R) 5′-CCTTGGTCCGTGT TTCAA GAC-3′ t° = 53 °C
	(VIII) LSU rDNA (part)	∼2,000 bp	(F) 5′-ACCCGCTGAAYTT AAGCATAT-3′ (R) 5′-AGCCAATCCTTWTCCCGAAG TTAC-3′ t° = 53 °C

[a]The sequence overlap between fragments I and II is about 480 bp, II and III—about 720 bp, III and IV—about 280 bp, IV and V—about 230 bp. The overlap between fragments VI and VII is about 180 bp, between VII and VIII—about 750 bp.

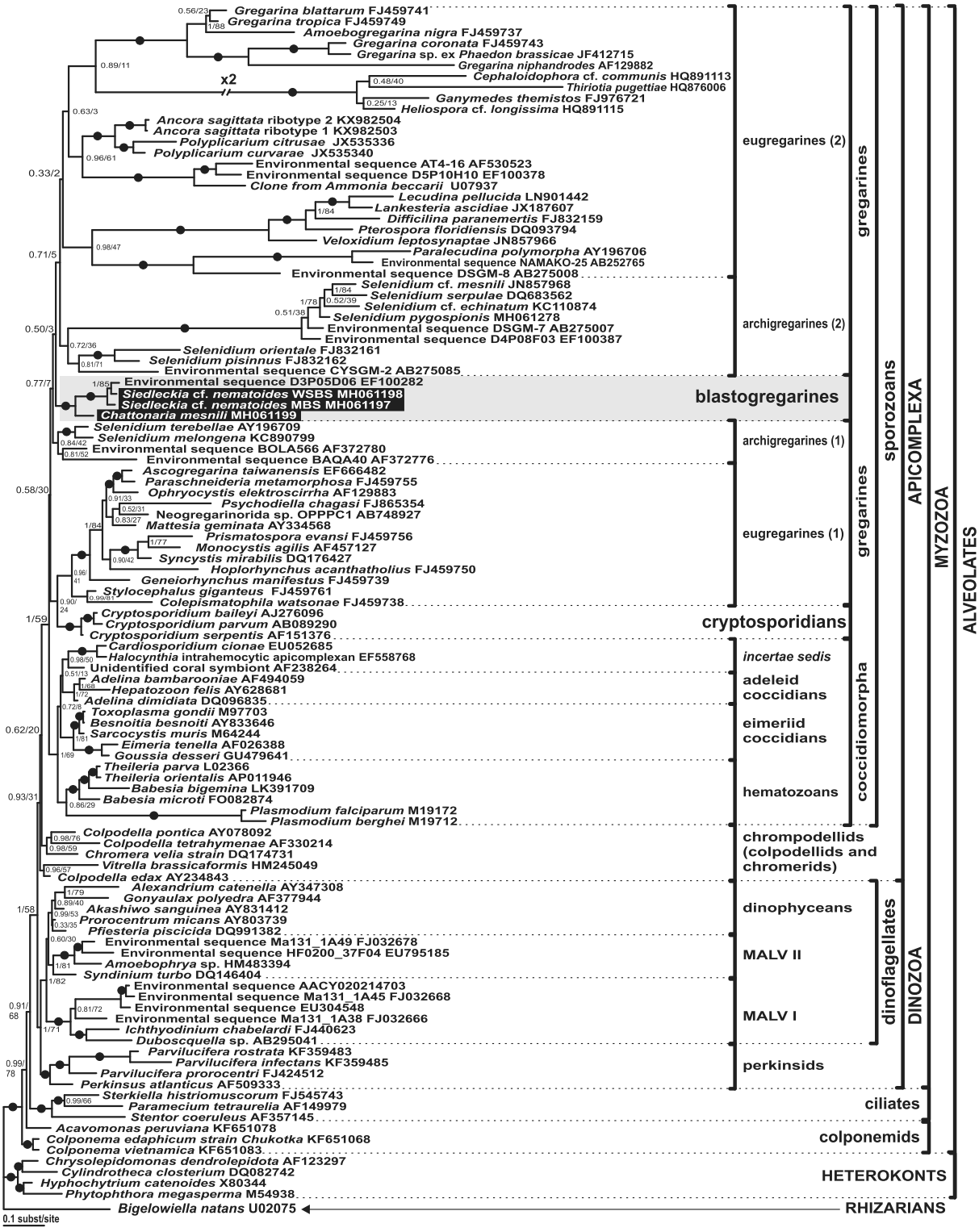

Figure 10. Bayesian inference tree of alveolates obtained by using the GTR + Γ + I model from the dataset of 110 SSU rDNA sequences (1,550 sites). Numbers at the nodes indicate Bayesian posterior probabilities (numerator) and ML bootstrap percentage (denominator). Black dots on the branches indicate Bayesian posterior probabilities and bootstrap percentages of 0.95 and 90%, respectively, and higher. The blastogregarine clade is highlighted by gray. The newly obtained sequences of blastogregarines (*Siedleckia nematoides* and *Chattonaria mesnili*) are given on black background.

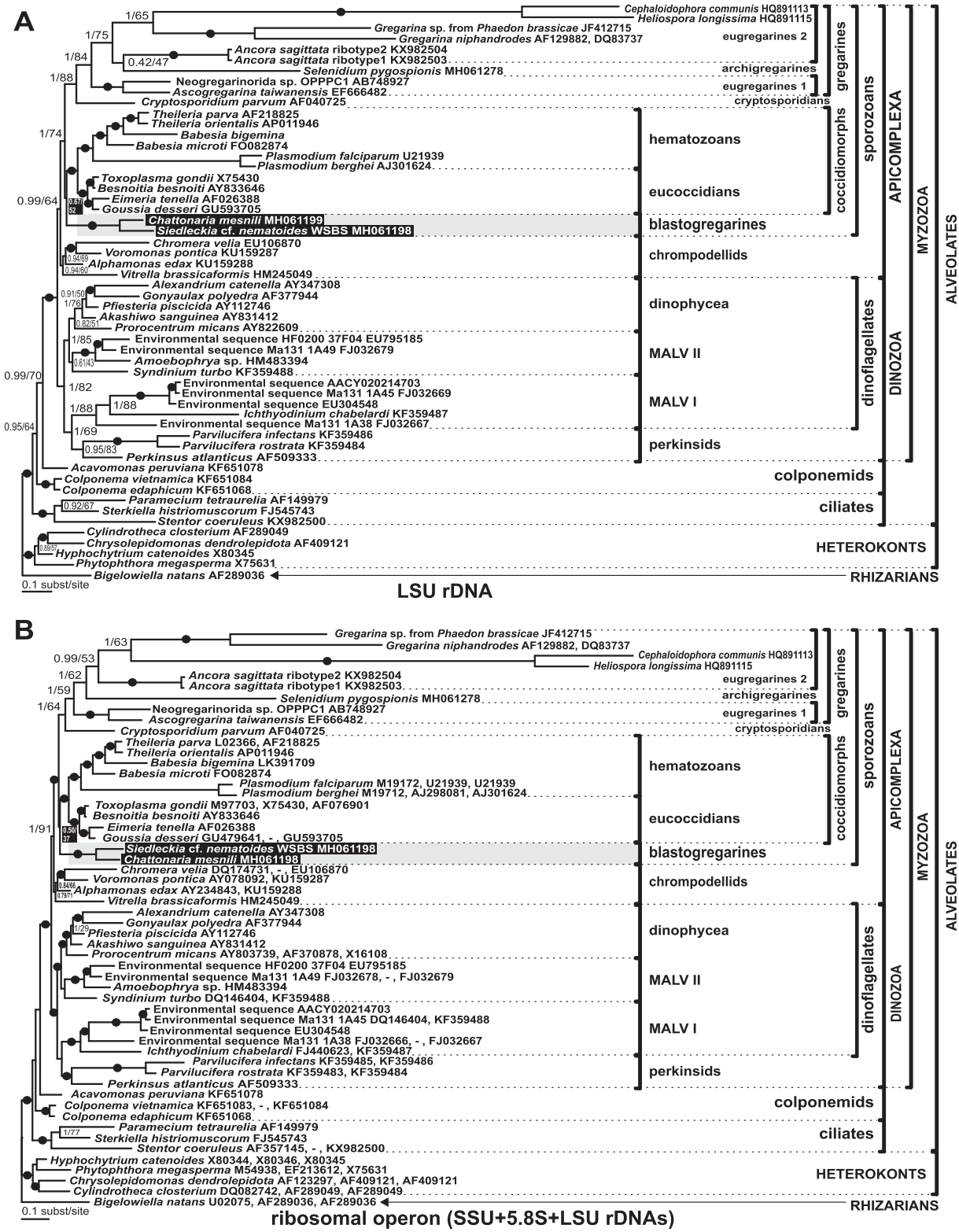

Figure 11. Bayesian inference trees of alveolates obtained by using the GTR + Γ + I model from two rDNA datasets of the same 54-taxon sampling. (**A**) LSU rDNA dataset (2,912 sites); (**B**) Ribosomal operon dataset (4,618 sites). Numbers at the nodes indicate Bayesian posterior probabilities (numerator) and ML bootstrap

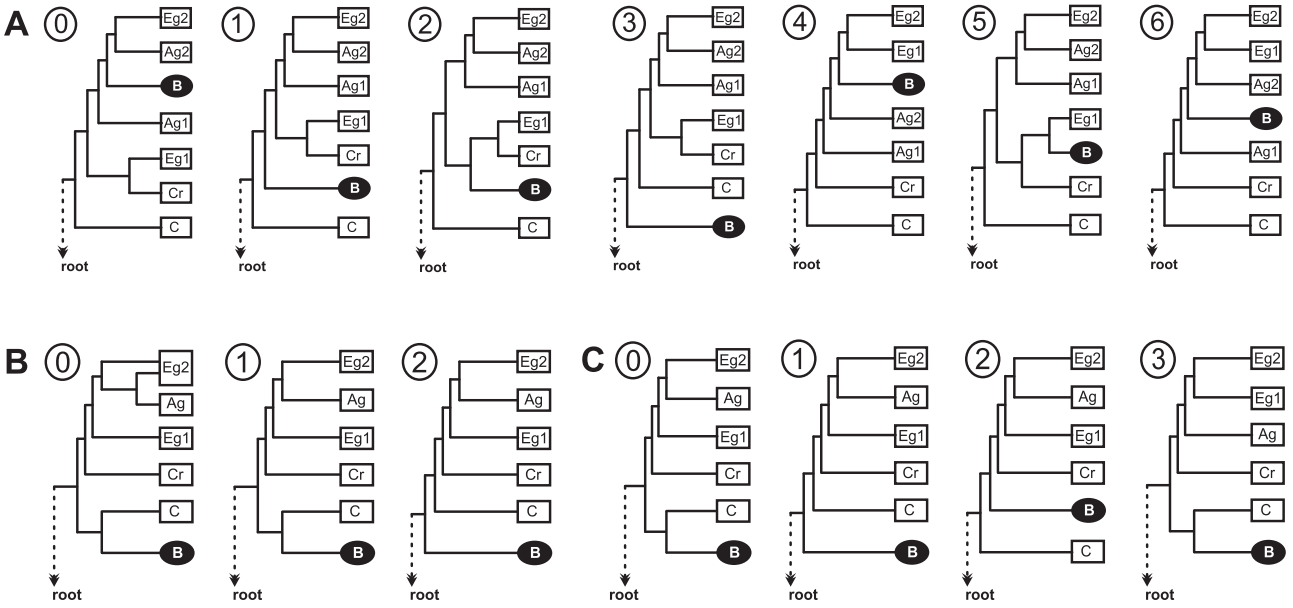

Figure 12. Diagrams of the reference ("best") phylogenies and alternative topologies rejected by none test: (**A**) SSU rDNA (110-taxon dataset); (**B**) LSU rDNA (54-taxon dataset); (**C**) ribosomal operon (54-taxon dataset). Only tree regions comprising parasitic apicomplexans are shown, the major clades correspond to those in the phylogenies obtained by the phylogenetic analyses (Figs 10 and 11) and are shown schematically. The reference trees are designated as (0). The alternative topologies are arranged from (1) and further on the decrease of the test values (see Table S3): the phylogenies having number (1) are the most likely of all alternative topologies in each category (A, B, C) and the last tree topologies are the least likely. Abbreviations: B, blastogregarines; Ag1 and 2, archigregarine clades (see Fig. 10); Eg1 and 2, eugregarine clades (see Figs 10 and 11); Cr, cryptosporidians; C, coccidiomorphs (coccidians + hematozoans). In the reference LSU rDNA phylogeny (B0) the archigregarine *Selenidium pygospionis* is grouped with the eugregarine *Ancora sagittata* belonging to the clade Eg2 in the phylogenies inferred from SSU rDNA and ribosomal operon (compare Figs 10 and 11), where they are separated; however, no one test did rejected they separation in the LSU rDNA phylogeny too (topology B1; the P-value of the AU test is even higher than for (0), see Supplementary Material Table S3).

primitive morphology of the mucron in this species could be the result of something like the paedomorphosis, i.e. the retention of "juvenile" features in an adult individual. The third common feature is shared by blastogregarines not only with archigregarines, but with all other gregarines too: their sporozoites lie in the oocysts freely (Chatton and Villeneuve 1936a), without additional internal cysts (sporocysts) characteristic for core coccidians, both eimeriids and adeleids; however, in some divergent blood-parasitic coccidians (e.g., *Lanketerella*) as well as in the majority of haemosporidians the sporocysts are absent too.

Apart from obvious similarities, there is a conspicuous difference between blastogregarine and archigregarine ultrastructure: the extensive development of the ER in the anterior half of the blastogregarine cell vs. secondary food vacuoles in the medullary part of the cytoplasm in the archigregarine cell (Schrével 1968, 1971b; Schrével et al. 2013; Simdyanov and Kuvardina 2007). One possible explanation for this is that the numerous nuclei in blastogregarines obstruct the traffic of food vacuoles along the axial microtubules from the mucron along the cell towards its rear. Such feeding mechanism was previously suggested for the archi-

percentage (denominator). Black dots on the branches indicate Bayesian posterior probabilities and bootstrap percentages of 0.95 and 90%, respectively, and higher. The blastogregarine clade is highlighted by gray. The newly obtained sequences of blastogregarines (*Siedleckia nematoides* and *Chattonaria mesnili*) are given on the black background. Accession numbers in (B) are arranged in following order: SSU rDNA, 5.8S (if exists), LSU rDNA.

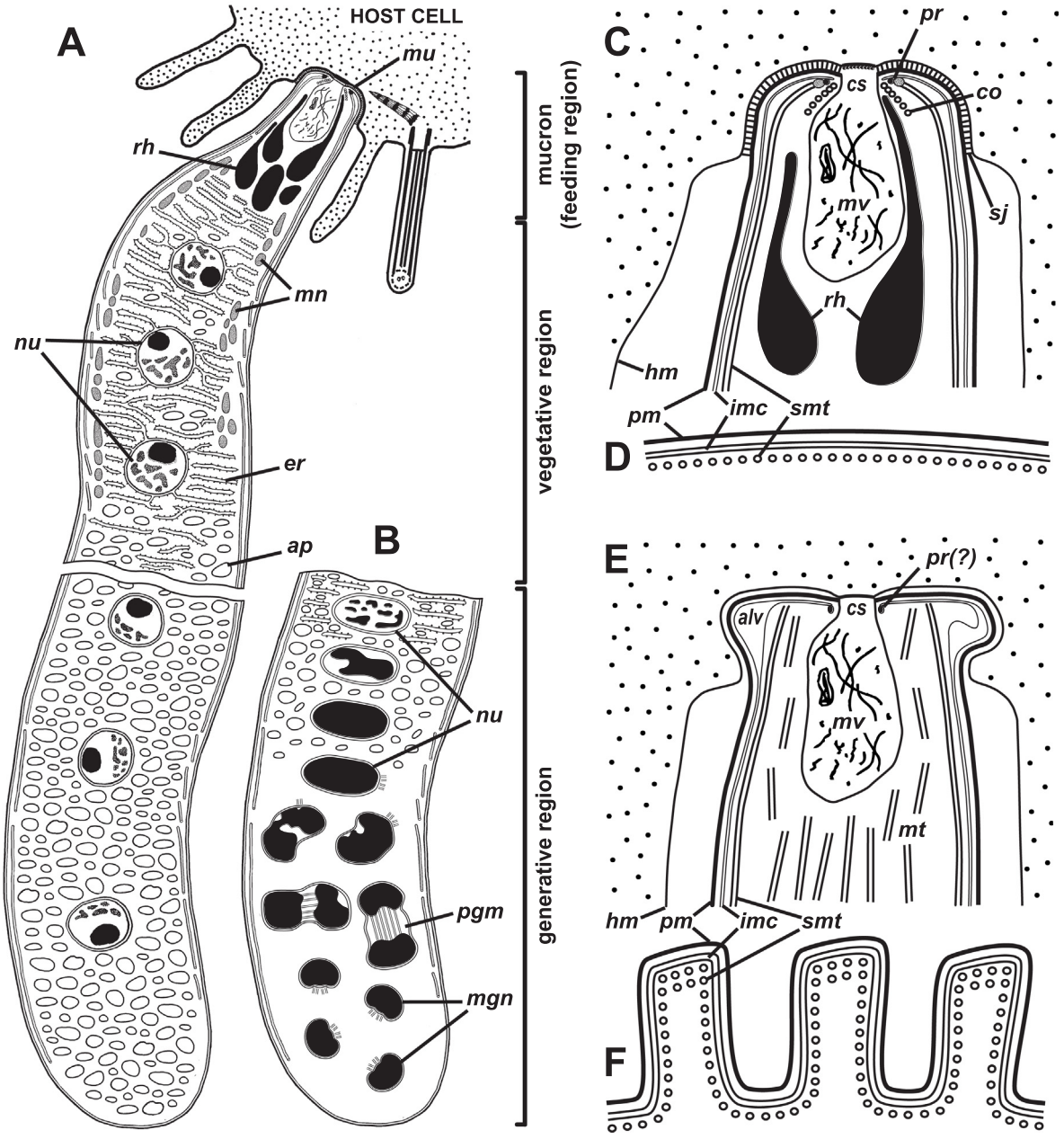

Figure 13. Key features of the organization of the blastogregarines. (**A**, **B)** Scheme of the general ultrastructure of a macrogamont cell and the egenerative region of a microgamont cell, respectively. (**C**, **D**) *Siedleckia nematoides*: the schemes of the longitudinal and cross sections of the mucron and tegument, respectively. (**E, F**) *Chattonaria mesnili*: the schemes of the longitudinal and cross sections of the mucron and tegument, respectively. Abbreviations: *alv*, alveoles between the cytomembranes of the IMC; *ap*, amylopectin granules; *co*, conoid; *cs*, cytostome; *er*, endoplasmic reticulum; *hm*, plasma membrane of the host cell; *imc*, inner membrane complex of pellicle; *pm*, plasma membrane; *mgn*, microgamete nuclei; *mt*, microtubules; *mv*, mucronal vacuole; *mu*, mucron; *nu*, nuclei; *pgm*, progamic mitoses in the microgamont; *pm*, plasma membrane of the parasite; *pr*, polar ring (gives rise to the longitudinal subpellicular microtubules (*smt*) in *Siedleckia*); *rh*, rhoptries; *sj*, septate cell junction between the parasite and host cells.

gregarine *Selenidium orientale* (Simdyanov and Kuvardina 2007). In the absence of that system, the ER may substitute the function of nutrient distribution. One more possible explanation is that the "overdeveloped" ER provides membranes necessary for blastogregarine budding.

On the other hand, the blastogregarines share some features with the coccidiomorphs that agrees with the topologies of the LSU rDNA and ribosomal operon phylogenies (although the blastogregarine position is also weakly supported there). First, like eimeriid coccidians and hematozoans, they lack one of the most characteristic features of the gregarine life-cycle: the stage of syzygy followed by the formation of the gametocyst (Grassé 1953a; Levine 1971; Perkins et al. 2000; Schrével and Desportes 2015; Schrével et al. 2013) – at least it was never reported in the literature and also did not detected by us throughout more than 10 years of observations. It should be noted here that the syzygy is characteristic not only for the gregarines, but for the adeleid coccidians too, but the gametocyst is still absent in them (Grassé 1953b; Perkins et al. 2000). Thus, the absent of the gametocyst is a common feature of the blastogregarines and coccidiomorphs. Second, judging by the two kinetosomes associated with the spermal nuclei, the male gametes (=microgametes) of blastogregarines must bear two flagella as in the majority of coccidians (Grassé 1953b; Perkins et al. 2000), whereas gregarine male gametes are chiefly uniflagellated or, sometimes (in Monocystidae), lack flagella at all (Grassé 1953a; Martinucci et al. 1981; Perkins et al. 2000; Schrével et al. 2013). Third, blastogregarines exhibit an extremely pronounced difference in size between male (micro-) and female (macro-) gametes (oogamy; Fig. 1H) that is a characteristic feature of all coccidians and haemosporidians (Chatton and Villeneuve 1936a). Thus, the atypical life cycle of blastogregarines is more similar to coccidians – as it was noted by Chatton and Villeneuve (1936b). For example, the multiple rounds of mitosis without immediate cytokinesis, that leads to multinuclearity (Fig. 1B–D), is characteristic not only for blastogregarines (Caullery and Mesnil 1899; Chatton and Dehorne 1929; Chatton and Villeneuve 1936a), but for the growing meronts of eucoccidians and haemosporidians too, e.g., in *Eimeria*, *Adelea*, and *Plasmodium* (Grassé 1953b; Perkins et al. 2000), although the multinuclearity is temporary in them. The only difference here is seemingly that these "merogonic" mitoses in blastogregarines do not result in the formation of merozoites (Chatton and Villeneuve 1936b).

The microgametogenesis of blastogregarines has not been traced, but the budding-off of already multinucleate spherical cells from microgamonts (Fig. 1E–F) has been previously reported for all examined blastogregarine species: *S.* cf. *nematoides*, *S. caullery*, and *S. mesnili* (Caullery and Mesnil 1899; Chatton and Dehorne 1929; Chatton and Villeneuve 1936a). These "buds" are supposed by Chatton and Dehorne (1929) to produce microgametes and, if so, they may be considered as microgametocytes or microgametoblasts – the latter is a peculiarity known in Protococcidia (e.g., *Myriospora*), which lack merogony (Grassé 1953b; Perkins et al. 2000). The formation of the microgametoblasts in blastogregarines and, probably, in the aforementioned protococcidians, may be considered as the deferred merogonic divisions of the cell. In blastogregarine macrogamonts, the suggested "deferred merogony" results in budding-off uninucleate putative macrogametocytes supposed to mature into macrogametes directly, i.e. without nuclear and cell divisions (again a coccidian feature) (Chatton and Dehorne 1929; Chatton and Villeneuve 1936a). To corroborate or dismiss these putative homologies in the blastogregarine and coccidian life cycles, the "asexual" nuclear divisions (not leading directly to the gamete formation) in the anterior part of the cell should be studied in details and the fate of these nuclei should be revealed: whether their "merogonic" divisions stop with the gamogony starting or they may continue within the lifespan of an individual. Another question is: whether the female nuclei really descend directly from the "asexual" (vegetative) nuclei of region 2 or there are additional progamic mitoses on the border between regions 2 and 3 as in microgamonts. The fate of the individuals after gametogenesis is also uncertain: whether they disintegrate totally during the gamete formation or the gametogenesis stops at some point and "merogonic" mitoses start again? Anyway, the merogonic (asexual) nuclear divisions and the formation of gamete nuclei appear to run in blastogregarines within the same cell, although in its different places – in region 2 and in region 3, respectively – therefore we introduce the name "merogamont" for blastogregarine individuals. The merogamont cell is differentiated into three regions specialized on different functions: mucron or feeding region (#1), merogonic or vegetative region (#2) where vegetative nuclei proliferate, and gamogonic or generative region (#3) where sexual (gametic, generative) nuclei arise and develop (Figs 2B, C; 3C, and 13).

Although the peculiarities of the nuclear apparatus and life cycle create a certain affinity between the blastogregarines and coccidians, the former also retain a set of plesiomorphic morphological characteristics shared with the archigregarines (see above), which should be therefore considered as common ancestral features of the sporozoans. Thus, we have two plesiomorphic groups of the Sporozoa with a quite similar organization, but one of them possesses the gregarine life cycle (archigregarines) while the other (blastogregarines) – the coccidia-like one. Summing up the morphological and molecular phylogenetic data, the blastogregarines should be considered as a relatively isolated group of plesiomorphic sporozoans. This conclusion appear to correlate with the results of the alternative topology testing that revealed the most basal position of blastogregarines within sporozoans as the only possible consensus between conflicting SSUrDNA and LSU rDNA ribosomal operon phylogenies. The mismatch of the "best" topologies might be referred to the twice less taxon sampling of LSU rDNA (54 vs. 110 taxa), but the comparison with the SSU rDNA trees computed on the reduced 54-taxon dataset (see Supplementary Material Fig. S2) showed the same features as in 110-taxon sampling SSU rDNA phylogeny: the split of gregarines and the affiliation blastogregarines to them. On the other hand, these reduced SSUrDNA phylogenies were considerably worse resolved and less consistent in the region of the apicomplexan backbone than both the LSU rDNA/operon-based trees (Fig. 11) and the SSU rDNA phylogenies inferred from the 110-taxon sampling (Fig. 10). This point rather corroborates the previously published opinion that SSU rDNA is likely not the most eligible marker for the study of apicomplexan deep branching (Simdyanov et al. 2015, 2017). The expanded taxon sampling of LSU rDNA and multigene analyses may resolve this ambiguity in the future.

Molecular phylogenetic analyses have failed to assign blastogregarines firmly to either gregarines or coccidiomorphs, but unequivocally indicate them as a robust clade affiliated to sporozoans that is in full agreement with the ultrastructural evidence. Apart from that, putative cryptic species within the morphospecies *S.* cf. *nematoides* were revealed by means of the molecular approach that may be inferred from significant differences between the sequences obtained from WSBS and MBS samples. The single available environmental blastogregarine-like sequence, D3P05D06 from oxygen-depleted sediment from littoral of Greenland (Stoeck et al. 2007), is also closely related to both sequences of *S.* cf. *nematoides*. To indicate these putative cryptic species more firmly, the molecular datasets must cover highly variable regions of the genome such as the internal transcribed spacers of the ribosomal operon, ITS1 and ITS2 (Müller et al. 2007). The hosts of the cryptic species might be cryptic species revealed within the *Scoloplos armiger* (Bleidorn et al. 2006) and the polychaetes closely related to it.

Conclusion

From all diversity of the contradicting to each other opinions reviewed in the Introduction, the results of this study corroborate the viewpoint on the taxonomic position of the blastogregarines of Chatton and co-authors and their pioneering interpretation of the blastogregarine life cycle (Chatton and Dehorne 1929; Chatton and Villeneuve 1936a,b) and dismiss the more recent and widespread taxonomic scheme of Levine and his followers, which consider blastogregarines a part of eugregarines (Levine 1985; Perkins et al. 2000; WoRMS). First, our ultrastructural data confirm the formation of microgamete nuclei in the formerly hypothetical microgamonts. Second, both molecular phylogenies and morphological data indicate that the blastogregarines definitely belong to the Apicomplexa and, more exactly, to the sporozoans. Third, molecular phylogenetic analyses fail to assign blastogregarines firmly either to the gregarines or coccidiomorphs (combined coccidians and hematozoans): these "best" SSU and LSU rDNA phylogenies conflict with each other and, additionally, are weakly supported in both cases; the morphological data reveal a plesiomorphic status blastogregarines as the relatively isolated group with the mixed features of coccidians and plesiomorphic gregarines. Proceeding from the aforesaid we classify the blastogregarines as a separate class Blastogregarinea (also see: de Puytorac et al. 1987) within the phylum Apicomplexa, subphylum Sporozoa. This class includes a single order Sidleckiida comprising two families, which separation from each other is based on the conspicuous differences in the structure of the attachment apparatus in *S.* cf. *nematoides* and *C. mesnili* manifested in the loss of the apical complex, change of the cell junction type, and development of additional attachment devices (alveolar bulge(s)) in the latter species. These differences are comparable with those between archi-

and eugregarines possessing mucron or epimerite, respectively, and this is in use as a relevant taxonomic criterion for the separation of the aforementioned orders within the genuine gregarines (Schrével and Desportes 2013a,b, 2015; Schrével et al. 2013; Simdyanov et al. 2017). Applying this morphological approach to the blastogregarines, however in the "limited mode" because of the sparsity of the group, we establish the new genus *Chattonaria* for *Siedleckia mesnili* (in honour of Édouard Chatton, who described this species and contributed significantly to the field of blastogregarine research), as well as the new family Chattonariidae, which, together with the family Siedleckiidae, compose the order Blastogregarinida, single in the class. We expect future increasing the species composition of the family Chattonariidae due to the addition of other named blastogregarine species as, e.g., *Siedleckia caulleryi* and the poorly described *S. dogieli*. Presumably, these organisms with longitudinal striations and complex attachment apparatus (as far as it may be inferred from light-microscopic data) can be members of the same genus *Chattonaria*. The composition of the family Siedleckiidae is expected to increase rather due to future recognizing cryptic species in the morphotype *S. nematoides* (see above). The consequent formal taxonomical actions are stated in the summary below.

Taxonomic Summary

Fixing the taxonomic position of the blastogregarines we leave the taxonomic ranks of Apicomplexa (phylum) and Sporozoa (subphylum) as originally established by Levine (Levine 1970, 1985; Levine et al. 1980) and update their diagnoses taking into consideration recent evidence.

Phylum APICOMPLEXA Levine, 1970

Diagnosis. The apical complex initially fulfilling myzocytosis and giving rise to longitudinal subpellicular microtubules arranged in layer(s); micropores.

Subphylum Sporozoa Leuckart, 1879 (Syn. Sporozoasida Levine, 1985)

Diagnosis. Parasitic Apicomplexa largely with the complex life cycle (Leuckart's triade) resulting in the oocysts performing sporogony and finally containing sporozoites; reduced plastid (apicoplast).

Class Blastogregarinea Chatton et Villeneuve, 1936, emend.

Diagnosis. Sporozoa. Epicellular parasites with permanent multinuclearity and gametogenesis: nuclear divisions of merogony and gamogony proceed within the same individual (merogamont) throughout its lifespan. The merogamonts with plesiomorphic ultrastructure: the well-developed apical (mucronal) complex performing myzocytotic feeding, regularly arranged longitudinal subpellicular microtubules arising from the mucron. The merogamonts are motile (bending), and sexually differentiated: in female individuals, the nuclei lie in a row along the cell axis, in male individuals they lie linearly only in the anterior part, but are scattered randomly in the posterior part of the cell. Oogamy is characteristic: female gamogony is realized by continuous budding of mononuclear macrogametocytes or macrogametes from the posterior part of female merogamonts, while male gamogony is realized by budding of multinuclear microgametocytes or microgametoblasts apparently followed by their dissociation into small putatively biflagellated male gametes with spermal nuclei. According to Chatton and co-workers (1929, 1936a) oocysts with many (10–16) free sporozoites (no sporocysts). Intestinal parasites of the polychaetes Orbiniidae.

Order Siedleckiida nom. nov.

With the characteristics of the class.

Family Siedleckiidae Chatton et Villeneuve, 1936, emend.

Diagnosis. With the characteristics of the order. Merogamonts with smooth surface lacking any grooves or folds. Mucron contains all components of the apical complex and performs myzocytotic feeding; apical ring(s) is likely MTOC of subpellicular microtubules. Monotypic.

Type genus. *Siedleckia* Caullery et Mesnil, 1898, emend.

Diagnosis. With the characteristics of the family. Merogamonts elongate and flattened with pointed anterior and rounded posterior ends. Monotypic, although the complex of cryptic species is suggested (molecular-phylogenetic data).

Type species. *Siedleckia nematoides* Caullery et Mesnil, 1898

Family Chattonariidae, fam. nov.

Diagnosis. With the caracteristics of the order. The mucron is modified: it performs myzocytotic feeding, but the apical complex is significantly reduced:

it retains only mucronal vacuole and, probably, polar ring, which is not connected with microtubules; no conoid and rhoptries. Monotypic.

Type genus. *Chattonaria*, gen. nov.

Diagnosis. With the characteristics of the family. Merogamonts elongate, cylindric, with roundly pointed posterior end; the surface with large longitudinal folds; mucron bearing voluminous alveoli with protuberances of the cytoplasm.

Type species. *Chattonaria mesnili* (Chatton et Dehorne, 1929), comb. nov. for *Siedleckia mesnili* Chatton et Dehorne, 1929

Etymology. Named in honour of Édouard Chatton, the eminent protistologist.

Note. *Siedleckia caulleryi* Chatton et Villeneuve, 1936 and *Siedleckia dogieli* Chatton et Dehorne, 1929 likely belong to the family Chattonariidae and to the genus *Chattonaria*, judging by their general morphology studied with LM. Ultrastructural and molecular-phylogenetic studies are required for a more precise conclusion. The species *S. dogieli* was established relying solely on a draft drawing by Dogiel with the indication of the host (Chatton and Dehorne 1929), i.e. it does not have a valid description and should be considered a nomen nudum.

Methods

Sampling: The hosts of *S.* cf. *nematoides* were collected from two littoral sites located in the Kandalaksha Gulf of the White Sea, Russia: on Bolshoy Gorely Island (66°18′46″N, 33°37′40″E) near Marine Biological Station of Saint Petersburg State University (MBS) and from the coast of Velikaya Salma Straight (66°33′11″N, 33°06′33″E) near White Sea Biological Station of Moscow State University (WSBS). The hosts of *Chattonaria mesnili* were collected on the lowest littoral zone of a sandy beach (48°41′23″N, 4°04′17″W) near Moguériec, coastal zone of English Channel, France.

The blastogregarine individuals were isolated by tearing apart the intestine of the hosts with fine tip needles under a stereomicroscope (MBS-1 or MBS-10 (LOMO, Russia) for *S.* cf. *nematoides*, or Olympus SZ40 (Olympus, Japan) for *C. mesnili*). The released parasites and small fragments of the host gut with the attached individuals were rinsed three times in filtered seawater using fine glass pipettes and then prepared for light microscopy (*S.* cf. *nematoides* only), scanning electron microscopy, transmission electron microscopy, and further DNA extraction.

Light microscopy: After rinsing in seawater, the living parasites were examined under light microscopes Leica DM2500, and Leica DM5000B (Leica Microsystems, Germany). Digital images of the living *S.* cf. *nematoides* were acquired under an MBR-1 microscope (LOMO, Russia) in phase-contrast mode with a Canon EOS 300D camera (Canon, Japan). Also wet smears of small pieces of the host intestine content were fixed by Bouin's fluid, stained by Böhmer's hematoxylin, and examined under a light microscope Zeiss AxioImager A1 with a digital camera AxioCam MRc5 (Carl Zeiss, Germany).

Electron microscopy: For SEM study, individual blastogregarines and small fragments of the host gut with attached blastogregarines were fixed with 2.5% (v/v) glutaraldehyde in 0.05 M cacodylate buffer (pH = 7.4) containing NaCl 1.28% (w/v) (for White Sea samples) or 2.3% (w/v) (for English Channel samples): two replacements of the fixative for 1 h each, in the ice bath in the dark, then rinsed three times (20 min each) with filtered seawater, and post-fixed with 2% (w/v) OsO_4 in the same buffer (room temperature, 2 h). Fragments of dissected gut containing the parasites were dehydrated in a graded series of ethanol up to 96% (v/v), transferred to a 96% ethanol/pure acetone mixture (1:1, v/v), rinsed three times with pure acetone, and critical point dried with CO_2. Alternatively, after 96% ethanol, the samples were rinsed three times with 100% ethanol and then critical point dried with CO_2. The samples were mounted on stubs, sputter coated with gold/palladium, and examined under a LEO-420 scanning electron microscope (Carl Zeiss, Germany) or a JSM-6380LA scanning electron microscope (JEOL, Japan).

The same fixation protocol as for SEM was used for the majority of TEM samples. To visualize the cell coat, some specimens of *S. cf. nematoides* were fixed with the mixture of glutaraldehyde and ruthenium red (3% (v/v) and 0.05% (w/v), respectively) in 0.2 M cacodylate buffer (pH = 7.4) and post-fixed with the mixture of OsO_4 and ruthenium red (1% (v/v) and 0.05% (w/v), respectively) in the same buffer – all under the same conditions as described above (Luft 1971a,b). After dehydration through ascending series of ethanol, the fixed samples were transferred into embedding mediums (Epon (Sigma-Aldrich, USA) or Spurr (Ted Pella, USA)) according to manufacturer's protocols, using acetone or isopropanol as intermediate dehydrating reagents for Epon and Spurr, respectively. Ultrathin sections (40 to 50 nm) were obtained using an LKB-III (LKB, Sweden), Reichert-Jung Ultracut E (C. Reichert, Austria) or Leica EM UC6 (Leica Microsystems, Germany) ultramicrotomes and then contrasted with uranyl acetate and lead citrate (Reynolds 1963) and examined under a JEM-100B, JEM-1010 or JEM-1011 electron microscopes (JEOL, Japan).

DNA isolation, PCR, cloning, and sequencing: After rinsing in seawater, blastogregarine individuals were collected into 1.5-ml microcentrifuge tubes: ~10 individuals of *S.* cf. *nematoides* from MBS (2003), ~100 individuals of *S.* cf. *nematoides* from WSBS (2004), and ~25 individuals *C. mesnili* (2010). For *S.* cf. *nematoides*, the material was lysed by an alkaline procedure (Floyd et al. 2002), and directly used for PCR amplification. For *C. mesnili*, the material was preserved in the "RNAlater" reagent (Life Technologies, USA), then stored at −20 °C until DNA extraction. The DNA extraction was performed using the "Diatom DNA Prep 200" kit (Isogen Laboratory, Russia). The resulting ribosomal DNA (rDNA) sequences were deduced from a combination of shorter fragments individually amplified using different pairs of primers (Table 1) and represented 18S or small subunit (SSU), 5.8S, 28S or large subunit (LSU) rDNAs, and internal transcribed spacers 1 and 2 (ITS 1 and ITS 2, respectively). All fragments were PCR amplified with an Encyclo PCR kit (Evrogen, Russia) in 25 μL of the reaction mixture prepared according to the manufacturer's protocol and contained 1 μL of the DNA extract using a DNA Engine Dyad thermocycler (Bio-Rad Laboratories, USA) and the following protocol: initial denatu-

ration at 95 °C for 3 min, 40 cycles of 95 °C for 30 s, 48 °C or 53 °C (see Table 1) for 30 s, and 72 °C for 1.5 min, and a final extension at 72 °C for 10 min. The PCR products of the expected size were cut from the gel and extracted by using a Cytokine DNA isolation kit (Cytokine, Russia). The PCR products were directly sequenced for fragments obtained from C. mesnili and *S.* cf. *nematoides* from MBS. The fragments obtained from *S.* cf. *nematoides* from WSBS were heterogeneous and therefore were cloned by using InsTAclone PCR Cloning Kit (Fermentas, Lithuania). Sequencing was performed using an ABI PRISM BigDye Terminator v. 3.1 reagent kit on an automatic sequencer Applied Biosystems 3730 DNA Analyzer (Applied Biosystems, USA). All sequences were tested with BLAST in order to detect the matches for apicomplexans and retain them for further analyses. For the sample of *S.* cf. *nematoides* from WSBS, the contiguous sequence of the near-completed ribosomal operon (SSU rDNA + ITS1 + 5.8S rDNA + ITS2 + LSU rDNA) was assembled from 5 overlapping PCR-amplified and cloned fragments, whereas only partial sequence of SSU rDNA alone was obtained from the sample of *S.* cf. *nematoides* from MBS. For the sample of *C. mesnili*, the assembled contiguous sequence (from 3 overlapped PCR-amplified fragments) covered near-complete gene of SSU rRNA, ITS1, 5.8S rDNA, ITS2, and a large part (~2,000 bp) of LSU rDNA (Table 1). The contiguous sequences were built with the use of BioEdit 7.0.9.0 (Hall 1999). The overlapped regions (180–750 sites, see Table 1) revealed 100% of matches. All obtained sequences were deposited in NCBI GenBank (accession numbers: MH061197-9).

Phylogenetic analyses: Three alignments were prepared for phylogenetic analyses: SSU rDNA (110 sequences, 1,550 sites), LSU rDNA (54 sequences, 2,913 sites), and the ribosomal operon (concatenated SSU, 5.8S, and LSU rDNAs: 54 sequencess, 4,618 sites). The alignments were generated in MUSCLE 3.6 (Edgar 2004) under default parameters and then manually adjusted with BioEdit 7.0.9.0 (Hall 1999); columns containing few nucleotides and hypervariable regions were removed. The taxon sampling of SSU rDNA alignment was designed in order to maximize the phylogenetic diversity and completeness of sequences in alignments, by preferentially selecting taxa having their SSU and LSU rDNA both sequenced. Representatives of heterokonts and rhizarians were used as outgroups.

The final alignment of SSU rDNA included 110 representative sequences (1,550 sites). To assess similarities among the SSU rDNA sequences within the blastogregarine clade, we calculated the percentage of identities as it is implemented in NCBI BLAST: the ratio of the matching sites to the total amount of unambiguous sites in the overlapping regions of each pair of aligned sequences: $b/a \times 100\%$, where a = total number of the aligned unambiguous sites, b = number of matches between them.

For the LSU rDNA and ribosomal operon (concatenated SSU, 5.8S and LSU rDNA sequences) analyses, the taxon sampling of only 54 sequences was used due to the limited availability of data for LSU rDNA, and, especially, 5.8S rDNA. Therefore, the 5.8S rDNA (155 sites in the alignment) was not represented in the analysis of concatenated rDNA genes for seven sequences (*Chromera velia*, *Colponema vietnamica*, *Goussia desseri*, *Stentor coeruleus*, and 3 environmental sequences: Ma131 1A38, Ma131 1A45, and Ma131 1A49): the corresponding positions were replaced with "N" in the alignment. The resulting multiple alignments contained 54 sequences (2,913 sites) for the LSU rDNA, and the same 54 sequences (4,618 sites) for the concatenated rDNAs (ribosomal operon). Thus, both taxon sampling comprised an identical set of species, all of which were also represented in the alignment of the 110 SSU rDNA sequences.

Maximum-likelihood (ML) analyses were performed with the RAxML 8.2.9 program (Stamatakis 2006) under the GTR + Γ model and CAT approximation (25 rate categories per site). The procedure included 100 alternative runs of the ML analysis and 1,000 replicates of multiparametric bootstrap. Bayesian inference (BI) analyses were conducted using MrBayes 3.2.6 program (Ronquist et al. 2012) under GTR + Γ + I model with 8 discrete categories of gamma distribution. The program was set to operate using the following parameters: nst = 6, ngammacat = 8, rates = invgamma, covarion = yes; parameters of Metropolis Coupling Markov Chains Monte Carlo (mcmc): nchains = 4, nruns = 4, temp = 0.2, ngen = 7,000,000, samplefreq = 1,000, burninfrac = 0.5 (first 50% of 7,000 sampled trees, i.e. first 3,500 generations were discarded in each run). The following average standard deviations of split frequencies were reached at the end of calculations: 0.009432 for the SSU rDNA analysis, 0.002976 for the LSU rDNA analysis, and 0.001371 for the ribosomal operon analysis.

Alternative tree topologies were manually created and edited using TreeView 1.6.6 program (Page 1996). The reference tree topology of SSU rDNA phylogeny (110-taxon dataset) was copied from the Bayesian tree (Fig. 10) that appeared more accurate in point of branching order within coccidiomorphs' clade (coccidians and hematozoans), but was identical with the corresponding ML tree in other respects. The reference topologies of LSU rDNA and ribosomal operons (54-taxon datasets) were copied from the trees showed in Figure 11; their ML and Bayesian phylogenies were identical. Alternative topologies were constructed by positioning the blastogregarines as a sister group successively to the major sporozoan clades, which were picked out as either high-resolved (high statistical supports) molecular phylogenetic lineages in the reference trees and published phylogenies or, in respect of low-resolved gregarines in SSU rDNA phylogenies, additionally relying on relevant morphological evidence (Simdyanov et al. 2017). As a result, we examined the relations of the blastogregarines to coccidiomorphs, cryptosporidians, different gegarine lineages, combined gregarine-cryptosporidian clade and sporozoa as a whole. Topology tests were performed with TREE-PUZZLE 5.3.rc16 and CONSEL 0.1j programs (Schmidt et al. 2002; Shimodaira and Hasegawa 2001). The following tests were used: Bootstrap Probability (Felsenstein 1985), Expected-Likelihood Weights (Strimmer and Rambaut 2002), Kishino-Hasegawa test (Kishino and Hasegawa 1989), Shimodaira-Hasegawa test (Shimodaira and Hasegawa 1999), Weighted Shimodaira-Hasegawa test (Shimodaira and Hasegawa 1999), and approximately unbiased test (Shimodaira 2002).

Acknowledgements

The authors thank the staff of the White Sea Biological Station of Lomonosov Moscow State University (WSBS MSU) and the Marine Biological Station of Saint Petersburg State University (MBS SPbSU) for providing facilities for field sampling and material processing. Light microscopic studies were conducted using equipment of the Center of microscopy WSBS MSU, Dept. of Invertebrate zoology of MSU, and Dept. of

Invertebrate zoology of SPbSU. Electron microscopic studies were performed in the Electron microscopy laboratory of the Faculty of Biology, Lomonosov Moscow State University (Russia), Center of Electron Miscroscopy of Papanin Institute for Biology of Inland Waters, Russian Academy of Sciences, Electron microscopy laboratory of Dresden Technical University (Germany), Research Recourse Centers of St Petersburg State University ("Molecular and Cell Technology" and "Environmental Safety Observatory"), and in Laboratory of Electron Microscopy of Institute of Parasitology, Academy of Sciences of the Czech Republic, České Budějovice. Authors are deeply grateful to the teams of these labs for technical support and help. This study used CYPRES Science Gateway (Miller et al. 2010) and the Supercomputer Center of Lomonosov Moscow State University (http://parallel.ru/cluster) to make phylogenetic computations. DNA sequencing was performed at the DNA sequencing center "Genome" (Engelhardt Institute of Molecular Biology, Russian Academy of Sciences, www.genome-centre.ru).

We would like to thank Kirill V. Mikhailov (Belozersky Institute of Physico-Chemical Biology, Lomonosov Moscow State University) for the assistance in several experiments and for his help in the calculations of sequence identities, Dr. Anna Zhadan (White Sea Biological Station) for her expert commentary on *Scoloplos* spp. biodiversity, and Dr. Nikolay Mugue (Institute of Developmental Biology, Russian Academy of Sciences) for his help in sequencing and valuable comments.

This work was supported by the Russian Foundation for Basic Research (projects No. 15-29-02601 and 18-04-00324), ECO-NET project 2131QM (Égide, France), the French governmental ANR Agency under ANR-10-LABX-0003 BCDiv, ANR-11-IDEX-0004-02, and ANR HAPAR (ANR-14-CE02-0007), the Interdisciplinary Program of the MNHN (ATM-Emergence des clades, des biotes et des cultures), and the Czech Science Foundation, project No. GBP505/12/G112 (ECIP). The phylogenetic analyses of SSU rDNA presented in this study were supported by the Russian Science Foundation, project No. 14-50-00029.

Appendix A. Supplementary Data

Supplementary data associated with this article can be found, in the online version, at https://doi.org/10.1016/j.protis.2018.04.006.

References

Adl SM, Simpson AG, Lane CE, Lukeš J, Bass D, Bowser SS, Brown M, Burki F, Dunthorn M, Hampl V, Heiss A, Hoppenrath M, Lara E, leGall L, Lynn DH, McManus H, Mitchell EAD, Mozley-Stanridge SE, Parfrey LW, Pawlowski J, Rueckert S, Shadwick L, Schoch C, Smirnov A, Spiegel FW (2012) The revised classification of eukaryotes. J Eukaryot Microbiol **59**:429–514

Alfaro ME, Zoller S, Lutzoni F (2003) Bayes or bootstrap? A simulation study comparing the performance of Bayesian Markov Chain Monte Carlo sampling and bootstrapping in assessing phylogenetic confidence. Mol Biol Evol **20**:255–266

Bleidorn C, Kruse I, Albrecht S, Bartolomaeus T (2006) Mitochondrial sequence data expose the putative cosmopolitan polychaete *Scoloplos armiger* (Annelida, Orbiniidae) as a species complex. BMC Evol Biol **6**:47

Caullery M, Mesnil F (1898) Sur un Sporozoaire aberrant (*Siedleckia* n. g.). CR Soc Biol **5**:1093–1095

Caullery M, Mesnil F (1899) Sur quelques parasites internes des Annelides. Trav Stat Zool Wimereux **7**:80–99

Cavalier-Smith T (2014) Gregarine site-heterogeneous 18S rDNA trees, revision of gregarine higher classification, and the evolutionary diversification of Sporozoa. Europ J Protistol **50**:472–495

Chatton E, Dehorne L (1929) Observations sur les Sporozoaires du genre *Siedleckia*. *S. dogieli*, n. sp. et *S. mesnili* n. sp. Arch Anat Microsc **25**:530–543

Chatton E, Villeneuve F (1936a) La sexualite et le cycle évolutif des Siedleckia d'apres l'étude de *S. caulleryi*, n. sp. Hologrégarines et Blastogrégarines. Sporozoaires Hologamétogènes et Blastogamétogènes. CR Acad Sci D Nat **203**:505–508

Chatton E, Villeneuve F (1936b) Le cycle évolutif de l' *Eleutheroschizon duboscqui* Brasil. Prevue expérimentale de l'absence de schizogonie chez la *Siedleckia caulleryi* Ch et Vill. CR Acad Sci D Nat **203**:834–837

Cox FEG (1994) The evolutionary expansion of the Sporozoa. Int J Parasitol **24**:1301–1316

Dogiel V (1910) Catenata. Organization of the genus *Haplozoon* and some forms similar to it. St Petersburg (In Russian)

Edgar RC (2004) MUSCLE: multiple sequence alignment with high accuracy and high throughput. Nucleic Acids Res **35**:1792–1797

Felsenstein J (1985) Confidence limits on phylogenies: an approach using the bootstrap. Evolution **39**:783–791

Floyd RM, Abebe E, Papert A, Blaxter ML (2002) Molecular barcodes for soil nematode identification. Mol Ecol **11**:839–850

Goggin CL, Barker SC (1993) Phylogenetic position of the genus *Perkinsus* (Protista, Apicomplexa) based on small subunit ribosomal RNA. Mol Biochem Parasitol **60**:65–70

Grassé P-P (1953a) Classe des Grégarinomorphes. In Grassé P-P (ed) Traité de Zoologie. Masson Paris, pp 550–690

Grassé P-P (1953b) Classe des Coccidiomorphes. In Grassé P-P (ed) Traité de Zoologie. Masson Paris, pp 691–797

Hall TA (1999) BioEdit: a user-friendly biological sequence alignment editor and analysis program for Windows 95/98/NT. Nucleic Acids Symp Ser **41**:95–98

Janouškovec J, Tikhonenkov DV, Burki F, Howe AT, Kolísko M, Mylnikov AP, Keeling PJ (2015) Factors mediating plastid dependency and the origins of parasitism in apicomplexans and their close relatives. Proc Natl Acad Sci USA **112**:10200–10207

Kishino H, Hasegawa M (1989) Evaluation of the maximum likelihood estimate of the evolutionary tree topologies from DNA sequence data, and the branching order in hominoidea. J Mol Evol **29**:170–179

Krylov MV, Dobrovolskij AA (1980) Macrosystem and phylogeny of the Sporozoa. In Krylov MV, Starobogatov YI (eds) Principles of the construction of the macrosystem of the unicellular animals. Academy of Sciences of the USSR Press, Leningrad, pp 62–74 (in Russian with English summary)

Kuvardina ON, Leander BS, Aleshin VV, Myl'nikov AP, Keeling PJ, Simdyanov TG (2002) The phylogeny of Colpodellids (Alveolata) using small subunit rRNA gene sequences suggests they are the free-living sister group to Apicomplexans. J Eukaryot Microbiol **49**:498–504

Leander BS (2008) Marine gregarines: evolutionary prelude to the apicomplexan radiation? Trends Parasitol **24**:60–67

Léger L (1909) Les Schizogregarines des Tracheates. II. Le genre *Schizocystis*. Arch Protistenkd **18**:5–15

Léger L, Duboscq O (1910) *Selenococcidium intermedium* Lég. et Dub. et la systématique des Sporozoaires. Arch Zool Exp Gen Ser **5**:187–238

Levine ND (1970) Taxonomy of the Sporozoa. J Parasit **56**:208–209

Levine ND (1971) Uniform terminology for the protozoan subphylum Apicomplexa. J Protozool **18**:352–355

Levine ND (1985) Phylum 2. Apicomplexa Levine, 1970. In Lee JJ, Hutner SH, Bovee EC (eds) An Illustrated Guide To The Protozoa. Society of Protozoologists, Kansas, pp 322–374

Levine ND, Corliss JO, Cox FEG, Deroux G, Grain J, Honigberg BM, Leedale GF, Loeblich AR, Lom J, Lynn D, Merinfeld EG, Page FC, Poljansky G, Sprague V, Vavra J, Wallace FG (1980) A newly revised classification of the Protozoa. J Protozool **27**:37–58

Lepelletier F, Karpov SA, Le Panse S, Bigeard E, Skovgaard A, Jeanthon C, Guillou L (2014) *Parvilucifera rostrata* sp. nov. (Perkinsozoa), a novel parasitoid that infects planktonic dinoflagellates. Protist **165**:31–49

Luft JH (1971a) Ruthenium red and violet. I. Chemistry, purification, methods of use for electron microscopy and mechanism of action. Anat Rec **171**:347–368

Luft JH (1971b) Ruthenium red and violet. II. Fine structural localization in animal tissues. Anat Rec **171**:369–415

Martinucci GB, Crespi P, Ferragosti E (1981) Contributions to the study of monocystid gregarines parasites of *Octolasium transpadanum*. III. Ultrastructural features of *Apolocystis* sp. gamonts, gametes and zygotes. Bolletino Zool **48**:243–253

Miller MA, Pfeiffer W, Schwartz T (2010) Creating the CIPRES Science Gateway for inference of large phylogenetic trees. Gateway Computing Environments Workshop (GCE), New Orleans, LA, pp 1–8

Müller T, Philippi N, Dandekar T, Schultz J, Wolf M (2007) Distinguishing species. RNA **13**:1469–1472

NCBI: National Center for Biotechnology Information. Available via https://www.ncbi.nlm.nih.gov.

Page RDM (1996) TREEVIEW: An application to display phylogenetic trees on personal computers. Comp Appl Biosci **12**:357–358

Perkins FO, Barta JR, Clopton RE, Peirce MA, Upton SJ (2000) Phylum Apicomplexa. In Lee JJ, Leedale GF, Bradbury P (eds) An Illustrated Guide to the Protozoa. Society of Protozoologists, Lawrence, KS (USA), pp 190–370

de Puytorac P, Grain J, Mignot J-P (1987) Précis de Protistologie. Societe Nouvelle des Editions Boubée, Paris, 581 p

Raikov IB (1982) The protozoan nucleus. Morphology and evolution. Springer, Vienna, New York, 474 p

Reynolds ES (1963) The use of lead citrate at high pH as an electron opaque stain in electron microscopy. J Cell Biol **17**:208–212

Rueckert S, Wakeman KC, Jenke-Kodama H, Leander BS (2015) Molecular systematics of marine gregarine apicomplexans from Pacific tunicates, with descriptions of five novel species of *Lankesteria*. Int J Syst Evol Microbiol **65**:2598–2614

Rueckert S, Horák A (2017) Archigregarines of the English Channel revisited: New molecular data on *Selenidium* species including early described and new species and the uncertainties of phylogenetic relationships. PLoS ONE **12**:e0187430

Ronquist F, Teslenko M, van der Mark P, Ayres DL, Darling A, Höhna S, Larget B, Liu L, Suchard MA, Huelsenbeck JP (2012) MrBayes 3. 2: Efficient Bayesian phylogenetic inference and model choice across a large model space. Syst Biol **61**:539–542

Schmidt HA, Strimmer K, Vingron M, von Haeseler A (2002) TREE-PUZZLE: maximum likelihood phylogenetic analysis using quartets and parallel computing. Bioinformatics **18**:502–504

Schrével J (1968) L'ultrastructure de la région antérieure de la Grégarine Selenidium et son interêt pour l'étude de la nutrition chez les Sporozoaires. J Microsc Paris **7**:391–410

Schrével J (1971a) Contribution à l'étude des Selenidiidae parasites d'Annélides Polychètes. II. Ultrastructure des quelques trophozoïtes. Protistologica **7**:101–130

Schrével J (1971b) Observations biologiques et ultrastructurales sur les Selenidiidae et leurs conséquences sur la systématique des Grégarinomorphes. J Protozool **18**:448–479

Schrével J, Desportes I (2013a) Introduction: Gregarines among Apicomlexa. In Desportes I, Schrével J (eds) Treatise on Zoology—Anatomy, Taxonomy, Biology. The Gregarines. Brill, Leiden, pp 7–24

Schrével J, Desportes I (2013b) Marine Gregarines. In Desportes I, Schrével J (eds) Treatise on Zoology—Anatomy, Taxonomy, Biology. The Gregarines. Brill, Leiden, pp 197–354

Schrével J, Desportes I (2015) Gregarines. In Mehlhorn H (ed) Encyclopedia of Parasitology. 4th edn Springer, Berlin, Heidelberg, pp 1–47

Schrével J, Desportes I, Goldstein S, Kuriyama R, Prensier G, Vávra J (2013) Biology of Gregarines and their Host-parasite Interactions. In Desportes I, Schrével J (eds) Treatise on Zoology—Anatomy, Taxonomy, Biology. The Gregarines. Brill, Leiden, pp 25–195

Schrével J, Valigurová A, Prensier G, Chambouvet A, Florent I, Guillou L (2016) Ultrastructure of *Selenidium pendula*, the type species of archigregarines, and phylogenetic relations to other marine Apicomplexa. Protist **167**:339–368

Shimodaira H (2002) An approximately unbiased test of phylogenetic tree selection. Syst Biol **51**:492–508

Shimodaira H, Hasegawa M (1999) Multiple comparisons of log-likelihoods with applications to phylogenetic inference. Mol Biol Evol **16**:1114–1116

Shimodaira H, Hasegawa M (2001) CONSEL: for assessing the confidence of phylogenetic tree selection. Bioinformatics **17**:1246–1247

Simdyanov TG (1992) *Selenidium pennatum* sp. n.—a new species of archigregarines from *Flabelligera affinis* (Polychaeta: Flabelligeridae). Parazitologiya **26**:344–347 (in Russian with English summary)

Simdyanov TG, Kuvardina ON (2007) Fine structure and putative feeding mechanism of the archigregarine *Selenidium orientale* (Apicomplexa: Gregarinomorpha). Europ J Protistol **43**:17–25

Simdyanov TG, Diakin AY, Aleoshin VV (2015) Ultrastructure and 28S rDNA phylogeny of two gregarines: *Cephaloidophora* cf. *communis* and *Heliospora* cf. *longissima* with remarks on gregarine morphology and phylogenetic analysis. Acta Protozool **54**:241–263

Simdyanov TG, Guillou L, Diakin AY, Mikhailov KV, Schrével J, Aleoshin VV (2017) A new view on the morphology and phylogeny of eugregarines suggested by the evidence from the gregarine *Ancora sagittata* (Leuckart, 1860) Labbé, 1899 (Apicomplexa: Eugregarinida). PeerJ **5**:e3354

Stamatakis A (2006) RAxML-VI-HPC: maximum likelihood-based phylogenetic analyses with thousands of taxa and mixed models. Bioinformatics **22**:2688–2690

Stoeck T, Kasper J, Bunge J, Leslin C, Ilyin V, Epstein S (2007) Protistan diversity in the Arctic: a case of paleoclimate shaping modern biodiversity? PLoS ONE **2**:e728

Strimmer K, Rambaut A (2002) Inferring confidence sets of possibly misspecified gene trees. Proc Roy Soc Lond B **269**:137–142

Théodoridès J (1984) The phylogeny of the Gregarinia (Sporozoa). Orig Life Evol Biosph **13**:339–342

Valigurová A, Vaškovicová N, Diakin A, Paskerova GG, Simdyanov TG, Kováčiková M (2017) Motility in blastogregarines (Apicomplexa): native and drug-induced organisation of *Siedleckia nematoides* cytoskeletal elements. PLoS ONE **12**:e0179709

Votýpka J, Modrý D, Oborník M, Šlapeta J, Lukeš J (2016) Apicomplexa. In Archibald J, Simpson A, Slamovits C (eds) Handbook of the Protists. Springer, Cham, pp 567–624

Wakeman KC, Horiguchi T (2017) Morphology and molecular phylogeny of the marine gregarine parasite *Selenidium oshoroense* n. sp. (Gregarina, Apicomplexa) isolated from a Northwest Pacific *Hydroides ezoensis* Okuda 1934 (Serpulidae, Polychaeta). Mar Biodivers, http://dx.doi.org/10.1007/s12526-017-0643-1

Wakeman KC, Leander BS (2013) Molecular phylogeny of marine gregarine parasites (Apicomplexa) from tube-forming polychaetes (Sabellariidae, Cirratulidae, and Serpulidae), including descriptions of two new species of *Selenidium*. J Eukaryot Microbiol **60**:514–525

Wakeman KC, Heintzelman MB, Leander BS (2014) Comparative ultrastructure and molecular phylogeny of *Selenidium melongena* n. sp. and *S. terebellae* Ray 1930 demonstrate niche partitioning in marine gregarine parasites (Apicomplexa). Protist **165**:493–511

WoRMS: World register of marine species. Available via https://www.marinespecies.org.